PCCP

Accepted Manuscript

This is an *Accepted Manuscript*, which has been through the Royal Society of Chemistry peer review process and has been accepted for publication.

Accepted Manuscripts are published online shortly after acceptance, before technical editing, formatting and proof reading. Using this free service, authors can make their results available to the community, in citable form, before we publish the edited article. We will replace this *Accepted Manuscript* with the edited and formatted *Advance Article* as soon as it is available.

You can find more information about *Accepted Manuscripts* in the **Information for Authors**.

Please note that technical editing may introduce minor changes to the text and/or graphics, which may alter content. The journal's standard **Terms & Conditions** and the **Ethical guidelines** still apply. In no event shall the Royal Society of Chemistry be held responsible for any errors or omissions in this *Accepted Manuscript* or any consequences arising from the use of any information it contains.

ROYAL SOCIETY OF CHEMISTRY

www.rsc.org/pccp

Exploring the glass transition region: crowding effect, nonergodicity and thermorheological complexity

Ashok K. Das*

School of Mechanical Engineering
Gyeongsang National University
Jinju, 660701, South Korea.

----
*Corresponding author
Email: akdas@gnu.ac.kr, akdas_vjti@yahoo.co.in
Phone: 82-55-772-2575
FAX: 82-55-772-1577

Abstract

Monte Carlo simulations performed on multiple polymer chains have produced accurate relaxation modulus $G_s(t)$ curves which match the experimental $G(t)$ curves of polystyrene reasonably well, over a wide temperature range around the glass transition region. The inter-segmental interactions, defined in terms of ε^* (well depth) and σ (monomer size), exert strong influence on the modulus, length scale and relaxation time scale of the system. Judicious selection of these interaction parameters has enabled us to create the whole range of temperature dependence of the thermorheological complexity, from $\Delta T = 40^0$ C to $\Delta T = 0^0$ C. Near the glass transition temperature, the development of nonergodicity *vis-à-vis* crowding effect in the system, emerge naturally from the analysis of the $G(t)$ line shapes. The entropic slow mode is well described by the Rouse theory and the energetic fast mode shifts to longer time scales, revealing the generic behavior of the thermorheological complexity. Typical $G_s(t)$ curves, when partitioned into the glassy and rubbery components, are shown to obey Inoue-Okamoto-Osaki's modified stress-optical rule, with different stress-optical coefficients for each component. Closer to the glass transition temperature, the distance of the closest monomer shows a considerable increase, suggesting a penetrable resistance to the approach of another monomer. The parameter σ represents the characteristic length scale of the system in the glassy region. The thermorheological complexity incorporates the dynamic length scale of the structural relaxation, increasing with the decrease of temperature towards the glass transition point.

Keywords:

Glassy relaxation; Entropic relaxation; Dynamical length scale; Modified stress-optical rule.

1. Introduction

Polymers are highly viscoelastic materials. Mechanical properties of polymeric substances vary widely depending on the duration and frequency of the applied stress. Any constitutive model on such viscoelastic substances is required to address the entire range of deformation behavior including linear viscoelastic as well as nonlinear viscoelastic responses. In the experiments, the response of the system is usually measured by the dynamic moduli $G'(\omega)$ and $G''(\omega)$ [or, simply the complex modulus, $G^*(\omega) = G'(\omega) + iG''(\omega)$], creep compliance $J(t)$ and relaxation modulus $G(t)$. Although all of the three responses may not be measured using a single instrument, the responses are interconvertible. For example, the creep compliance $J(t)$ and relaxation modulus $G(t)$ are related by a convolution integral as[1]

$$t = \int_0^t J(t-\tau)G(\tau)d\tau = \int_0^t G(t-\tau)J(\tau)d\tau$$

Similarly, both the dynamic moduli $G'(\omega)$ and $G''(\omega)$ can be expressed as analytical functions in terms of the relaxation modulus $G(t)$ and creep compliance $J(t)$.[2] The time-temperature superposition principle[3-5] is a general tool for the description of viscoelastic behavior of linear polymers over a wide range of time (or, frequency). The temperature dependence of the viscoelastic response of a polymer melt incorporates a short-time (high frequency) and a long-time (low frequency) region. The high frequency region is usually known as the glassy, structural or α-relaxation while the low frequency region constitutes the entropic counterpart. As the temperature approaches the glass transition point (T_g), the relative increase in the modulus in the glassy region becomes larger than the corresponding increase in the entropic region.[6-14] As a consequence, the time-temperature superposition principle would not be applicable over the whole range of time

3

(or, frequency), preventing the construction of the so-called 'master curve'. This is generally referred to as the thermorheological complexity.

For the purpose of constructing a master curve, one needs to calculate a horizontal shift factor a_T and a vertical shift factor b_T, both of which are temperature dependent. While the vertical shift factor is related to the temperature dependent density of the system, the horizontal shift factor is often calculated from the Williams-Landel-Ferry (WLF) equation[15] for temperatures above the T_g. The close relationship between the changes in viscoelastic response with temperature near the glass transition point has been well recognized in literature, but the thermorheological complexity has not been included in any theoretical considerations.[16-18]

At temperatures close to the T_g, nonergodicity in the system plays an important role in the fast relaxation mode, but in the long-time region (entropic mode) the ergodicity is recovered.[19] The ergodic behavior of a polymeric system implies that different modes of motion (such as the Rouse normal modes) are characterized by the same frictional factor. As the frictional factor carries the temperature dependence of all the entropy driven processes, it can be used to normalize the glassy relaxation time, whose temperature dependence is much stronger. The ratio of the average glassy relaxation time (τ_G) to the frictional factor (K) can be estimated as a function of temperature. The glassy relaxation process which involves a 'large length scale dynamics' may then be characterized by this ratio, (τ_G/K). Importance of such a scheme of analysis is highly relevant as the nonergodic dynamic process in the short-time region must eventually fade into the fully ergodic process in the long-time region.[19]

Quantitatively successful theories based on models using coarse-grained structural units (viz.,

the Rouse segments) have been developed in order to explain the viscoelastic response in the

intermediate time and long time region.[20-24] For a phenomenological description of the short-time

(glassy) relaxation, one may employ the Kohlrausch-Williams-Watts' (KWW) stretched

exponential function.[25] The empirical KWW form assumed for the glassy relaxation is

incorporated into the molecular theory. In certain cases, the use of a single KWW function may

not be sufficient for precisely describing the whole glassy relaxation, which may comprise

processes with more than one relaxation times.[26]

For the entanglement-free cases, Lin and Das[27,28] have calculated the linear and nonlinear

stress relaxations using single Fraenkel chains, with explicitly skeletal bonded interactions.

Considering a mean field of interactions for the single chains, the MC simulations on

entanglement-free polymer melts revealed the emergence of two distinct dynamic modes in the

relaxation modulus $G_s(t)$ curves. Detailed analyses confirmed that the fast mode arises from the

segment-tension fluctuations (an energetic interactions-driven process) while the slow mode

originates from the randomization of the segmental orientations (an entropy-driven process).

Furthermore, the slow mode is well described by the Rouse theory in all respects: modulus level,

time scale and the line shape. This leads to infer that, one Fraenkel bond segment can substitute

for one Rouse segment, suggesting that the entropic force constant of the bond segment is not a

prerequisite for giving rise to the Rouse behavior. A Fraenkel segment with a sufficiently large

force constant is equivalent to a Kuhn segment, as far as the chain conformation is concerned. This

conclusion has resolved a long-standing debate on the success of the Rouse segment-based theories

on polymer viscoelasticity.[29] In essence, the overall two-mode line shape of the simulated $G_s(t)$ is

in good agreement with the experimental curve for an ideally monodisperse sample. The agreement suggests that the amazingly simple Fraenkel chain model captures the basic element (namely, the rigidity of the segment) of the energetic interactions in the polymer system and represents a dramatic improvement on the Rouse model. However, as the Fraenkel chain is still somewhat primitive, it is not expected to describe the fast mode precisely; both the modulus level and the relaxation in the fast mode region depend on the Fraenkel force constant (H_F). The details regarding the choice of H_F to be used in the MC simulations presented in this article, have been explained in Appendix I.

It is noteworthy that the inter-segmental interactions (ISI) exert strong influence on the $G_s(t)$ line shape in the fast mode region. In the single Fraenkel chain simulations, the interactions between segments (intermolecular and intramolecular) in a polymer have been implicitly related to a mean interactions field and these are absorbed in the fluctuating step movements, dictated by the fluctuating forces acting on each bead of the chain.

The present article focuses on further development in the framework on the emergence of the bimodal relaxation behavior from the MC simulations of the Fraenkel chains. In the present multiple chain systems, each bead interacts with all non-nearest beads in the same chain and all beads of the other chains through a modified Lennard-Jones (LJ) potential. With a view to fitting the simulation data to experiments, $H_F^*(= H_F/k_BT) = 600$ is chosen in the present study. The change in the Fraenkel force constant does not affect the validity of the simulation results. Changes in the $G_s(t)$ line shapes as a function of the LJ potential parameters $\varepsilon^*(= \varepsilon/k_BT)$ (well depth) and σ (bead diameter) have been investigated in detail. The generic structure-property relationship in the polymer system has unraveled the cause of the observed thermorheological complexity. The

structural parameters (obtained from optimal fitting of the simulation data to the experimental $G(t)$ curves at different temperatures) are found to be more than satisfactory to account for the thermorheological complexity in the homopolymer system, around the glass transition point.

The rest of the article has been organized as follows. We have presented the methodology of the simulations and the scheme for data analysis in Section 2. Results and discussion have been presented in Section 3, revealing the importance of the parameters ε^* and σ in dictating the relaxation behavior in the entire time region. The said parameters have been optimized so as to match the simulation $G_s(t)$ data with the experimental $G(t)$ line shapes of a monodisperse polystyrene sample. The applicability of the modified stress-optical rule (MSOR) has been verified by partitioning the simulation $G_s(t)$ into contributions due to the glassy behavior and rubbery state, with different stress-optical coefficients for each. Thermorheological complexity emerges as a natural phenomenon as the temperature is lowered towards the T_g of the system. The requirement of a longer length scale at the T_g has been fulfilled by a larger value of the σ parameter. A critical discussion on the thermorheological complexity around the T_g has also been included. Section 4 lists the conclusions from the study and outlines possible avenues which need to be explored in the future.

2. Methodology

For the purpose of calculating the relaxation modulus curves for the polymeric system, we construct the coarse-gained systems consisting of c chains, each with N beads. The chains have been modeled as bead-spring chains of LJ particles interacting through the Fraenkel potential[30] (for the bead-bead backbone) and the modified LJ potential for the non-neighbor beads. As the

main interest of this article is to recreate the thermorheological complexity, we have considered

multiple chains whose center of mass (COM) positions are confined in a cubic simulation box of

edge length L. During the Monte Carlo simulation of these systems, periodic boundary conditions[31]

have been applied, based on the position of the COM of each chain. Initial configurations of chains

of N beads have been generated as follows.[32,33] Taking the first bead as the seed (placed arbitrarily

at the origin), coordinates (x_i, y_i, z_i) of the successive beads are generated using,

$x_i = x_{i-1} + \sigma \sin\theta \cos\phi$; $y_i = y_{i-1} + \sigma \sin\theta \sin\phi$; $z_i = z_{i-1} + \sigma \cos\theta$; for i = 2, 3, ..., N; angles θ

and ϕ are obtained from $\theta = \pi * qq$ and $\phi = 2\pi * ff$ respectively, where qq and ff are two random

numbers generated for each bead. Consecutive inter-bead distances are matched with σ, before

accepting the coordinates of the new bead to build the chain. Once the first N-beads chain has been

made, its COM is calculated and the chain is placed inside the cubic box. The second chain of the

system was placed into the box in such a way that the COM of the second chain is at a radial

distance of σ from the COM of the first. The placement of the subsequent chains was done in a

similar manner, avoiding overlap of the COMs. Each simulation box contains 16 chains, each with

20 beads. Each system was then equilibrated for 10^5 MC steps during which several physical

quantities were monitored. The production runs comprise another 10^5 MC steps on the equilibrated

configurations.

For the bead-bead backbone, each bead interacts with its nearest neighbors in the same chain

through the Fraenkel potential.[30]

$$V_{\text{Fraenkel}}(r) = \frac{H_F}{2}(r - b_0)^2 \qquad (1)$$

where, H_F is the force constant and b_0 is the equilibrium bead-bead distance. Each bead of the

chain interacts with all non-nearest neighbor beads in the same chain and all beads of the other

chains through the modified LJ potential as defined below. The LJ interactions are truncated and shifted to zero beyond a cutoff, $r_c = 2 * (2)^{1/6} \sigma = 2.245 \sigma$. If the distance between two beads i and j is denoted by, $r_{ij} = (r_i - r_j)$ with $\{\mathbf{r}_i\}$ as the position vectors, the modified LJ potential is defined by,

$$V_{\text{LJ}}(r_{ij}) = 4\epsilon \left[\left(\frac{\sigma}{r_{ij}} \right)^{12} - \left(\frac{\sigma}{r_{ij}} \right)^{6} \right], \text{ for } r_{ij} < 2 * (2)^{1/6} \sigma \qquad (2a)$$

$$V_{\text{LJ}}(r_{ij}) = 0, \text{ for } r_{ij} \geq 2 * (2)^{1/6} \qquad (2b)$$

where, σ is the diameter of a bead and ε is the energy parameter representing the depth of the potential. In the literature, a more familiar bonded interactions is the finitely extensible nonlinear elastic (FENE) potential function.[34] For the simulation of the multiple polymer chain system, we have chosen the Fraenkel + LJ combination over the FENE + LJ combination. Although the latter is more frequently used in polymer simulations, it is asymmetric with respect to the equilibrium bond length (= 0.96σ).[35] The Fraenkel + LJ combination does not have any appreciable asymmetry around the potential minimum, as shown earlier.[32]

We have set the thermal energy, $k_B T = 1$ for the simulations (k_B is the Boltzmann constant and T is the absolute temperature). Thus, the energy parameters such as $H_F^*(= H_F / k_B T)$ and $\varepsilon^*(= \varepsilon / k_B T)$ have the unit of $k_B T = 1$ implicit on them. For the simulations, we have set $b_0 = 1$ and the bead diameter σ is varied in the range from 0.08 to 0.65.

In the Langevin dynamics method, motion of each bead of the chain is governed by the total force on the bead, which comprises of force arising from potential, a frictional force and a random force.[33]

$$\mathbf{F}_i^{Total} = m_i \frac{d^2 \mathbf{r}_i}{dt^2} = \mathbf{F}_i^C + \mathbf{F}_i^F + \mathbf{F}_i^R \qquad (3)$$

where, m_i is the mass of the bead. The force arising from the chosen Fraenkel + modified LJ potential are included in $\mathbf{F}_i^C$. The frictional force acting on the bead is, $\mathbf{F}_i^F = -\xi\mathbf{v}_i$, where $\mathbf{v}_i$ is the velocity of the bead and ξ is the friction coefficient. The friction coefficient ξ is related to the fluctuations of the random force, $\mathbf{F}_i^R$ through the fluctuation-dissipation theorem,[36]

$$\left\langle \mathbf{F}_i^R(t) \right\rangle = 0 \tag{4a}$$

$$\left\langle \mathbf{F}_i^R(t) \cdot \mathbf{F}_j^R(t') \right\rangle = 6k_{\mathrm{B}}T\xi\delta_{ij}\delta(t-t') \tag{4b}$$

where, k_{B} is the Boltzmann constant and T is the absolute temperature of the system.

In the MC simulations, the continuous change in time, dt, is replaced by a small time step, Δt. If the position of the beads at a time step t is denoted by $\{\mathbf{r}_i(t)\}$, the bead positions at the next time step $(t + \Delta t)$ is given by,[27,28,33]

$$\mathbf{r}_i(t + \Delta t) = \mathbf{r}_i(t) + \left(\frac{d^2}{2k_{\mathrm{B}}T}\right)\mathbf{F}_i^{Total}(t) + \mathbf{d}_i(t) \tag{5}$$

where, $\mathbf{F}_i^{Total}(t)$ is the total force exerted on the bead. The random step vector, $\mathbf{d}_i(t)$ is characterized by its first and second moments,

$$\langle \mathbf{d}_i(t) \rangle = 0 \tag{6a}$$

$$\langle \mathbf{d}_i(t)\mathbf{d}_j(t') \rangle = d^2 \mathbf{I}\delta_{ij}\delta(t-t') \tag{6b}$$

where, $\mathbf{I}$ is a unit tensor.

The random displacement d, and time step Δt, are related through the diffusion constant D, of the chain[27,28,32,33]

$$d^2 = 2D\Delta t = \frac{2k_{\mathrm{B}}T\Delta t}{\xi} \tag{7}$$

The friction coefficient (ξ) is dependent on the collision frequency (γ) by, $\gamma = \left(\xi/m_i\right)$. The

quantity γ^{-1} can be considered as the time taken by the particle to lose memory of its initial velocity

(or, γ^{-1} is the 'velocity relaxation time' of the particle).[37] Therefore, eq. (5) and (7) are not in

conflict with eq. (3) as the friction coefficient ξ contains the implicit dependence on bead mass m_i.

One may rewrite eq. (5) as,

$$\mathbf{r}_i(t + \Delta t) = \mathbf{r}_i(t) + \frac{\Delta t}{\xi}\, \mathbf{F}_i^{Total}(t) + \mathbf{d}_i(t) = \mathbf{r}_i(t) + \frac{\Delta t}{\gamma m_i}\mathbf{F}_i^{Total}(t) + \mathbf{d}_i(t) \tag{8}$$

When the velocity relaxation time (γ^{-1}) is much smaller than the integration time step (Δt), the

motion is diffusive, and the interparticle force is assumed to be constant over Δt. [See also Eq.

(7.121) in Ref. 37].

The relaxation times of the (Fraenkel + modified LJ) chains need to be compared with those

of the Rouse chains, for which exact analytical expressions are known.[20,33,38] During the

simulations, the periodic boundary conditions[31] have been applied on the COM of the chains. This

involves calculation of the COM at each simulation step; if the location of the COM is outside of

the box, the whole chain is converted into its periodic image. Unlike in the simulation of systems

comprising of small molecules, a considerable number of beads of the chains may lie outside of

the cubic box. This does not cause problems in calculating the modified LJ forces on these beads,

as the minimum image distance[31] between any two beads is automatically used in calculating the

interaction forces.

We consider a sample of polymer melt placed between two parallel plates such that the adhesion between the sample and the plates is strong enough that there is no slippage at either surface. For simple shear applied on a perfectly elastic sample, the shear stress and the shear strain are linearly related and the constant of proportionality is known as the shear modulus.[33,39] In the case of a step-strain deformation applied on a viscoelastic material, the stress after such a step-strain will have some general time dependence and the stress relaxation modulus is calculated as the ratio of the stress remaining at that instant and the magnitude of the step-strain applied.[39] In order to obtain $G(t)$ by simulation, one may consider the polymer chain of N beads to be subjected to a shear deformation $\mathbf{E}$ at time $t = 0$.[27,28,33]

$$\mathbf{E} = \begin{pmatrix} 1 & \lambda & 0 \\ 0 & 1 & 0 \\ 0 & 0 & 1 \end{pmatrix} \tag{9}$$

For linear viscoelasticity, λ should be small ($\lambda \to 0$). This has been implemented in the simulations as below. At time $t = 0$, the coordinates of the ith bead are transformed as,

$$\begin{pmatrix} x_i' \\ y_i' \\ z_i' \end{pmatrix} = \begin{pmatrix} 1 & \lambda & 0 \\ 0 & 1 & 0 \\ 0 & 0 & 1 \end{pmatrix} \begin{pmatrix} x_i \\ y_i \\ z_i \end{pmatrix} \tag{10}$$

The evolution of the bead positions may then be calculated through the Langevin equation of motion. By making use of the Kramers-Kirkwood expressions for stress tensor,[40,41] we may write the relaxation modulus of the sample as,[27,28,33]

$$G_s(t) = \frac{1}{6(N-1)} \sum_{\alpha \neq \beta} \left\langle J_{\alpha\beta}(0) J_{\alpha\beta}(t) \right\rangle \tag{11}$$

with $J_{\alpha\beta}(t) = \sum_{i=1}^{N} F_{i\alpha}(t)\beta_i(t)$ and $\alpha, \beta \equiv x, y, z$ ($\alpha \neq \beta$ for calculating $J_{\alpha\beta}$). The angular brackets signify the average over all the relaxation processes considered.

The present study is devoted to examine the viscoelastic responses of the polymer melts. In spite of the differences that exist between the equilibrium and step-strain simulations in the relaxation behavior in the fast mode region, we use the equilibrium simulations in this study. The reasons have been explained in Appendix II.

3. Results and Discussion

3.1. Contribution of the inter-segmental interactions (ISI) to the $G_s(t)$

The $G_s(t)$ line shapes obtained from the simulations of the multiple chain (16 chains $\times$ 20 beads) systems using the Fraenkel + modified LJ interactions (open circles) for $\varepsilon^* = 0.05$, 0.10 and 0.15; σ fixed at 0.25 are presented in Figure 1. In order to compare, the results of single 20-bead Fraenkel chains as single chain (open squares) and multiple chain (16 chains $\times$ 20 beads) systems using only the Fraenkel force (open triangles) are also shown. The three types of $G_s(t)$ curves are finally compared with the Rouse analytical curves (solid lines). These are identified as $mcTG_s(t)$, $scG_s(t)$, $mcFG_s(t)$ and Rouse$G_s(t)$, respectively [$mcT \equiv$ multiple chain using total force, $sc \equiv$ single chain, $mcF \equiv$ multiple chain using only Fraenkel force]. For the sake of clarity, the $\varepsilon^* = 0.10$ and 0.15 family of curves are shifted vertically by two and four decades, respectively.
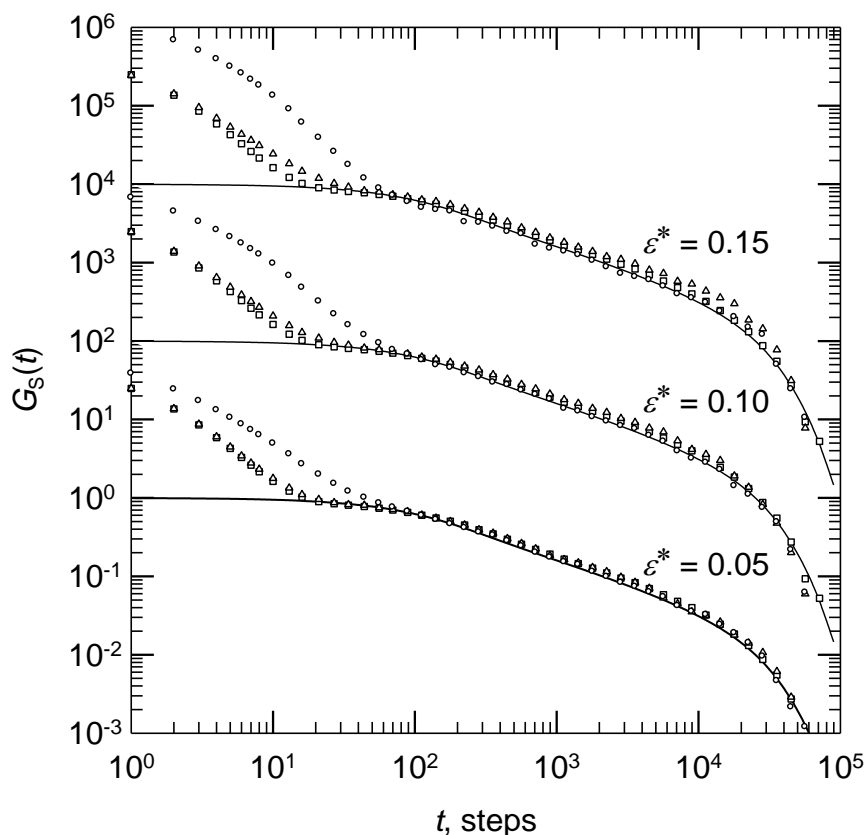
Figure 1: Comparison of the simulation $G_s(t)$ curves at three different $\varepsilon^* = 0.05$, 0.10 and 0.15 and with σ fixed at 0.25. Results for 16 chains × 20 beads, Fraenkel + modified LJ: $mcTG_s(t)$: (O), total force being used in stress calculations; 1 chain × 20 beads, Fraenkel: $scG_s(t)$: (□); 16 chains × 20 beads, Fraenkel + modified LJ: $mcFG_s(t)$: (Δ), only the Fraenkel force being used in stress calculations. Also shown are the Rouse analytical curves (——) Rouse$G_s(t)$, for $N = 20$. To avoid overlapping, the families of curves at $\varepsilon^* = 0.10$ and 0.15 have been shifted vertically by 2 decades and 4 decades, respectively.

It can be seen from Figure 1 that a close superposition of the $mcTG_s(t)$, $scG_s(t)$ and $mcFG_s(t)$ simulation data over the analytical Rouse$G_s(t)$ data occur at the slow mode region without any shift in either the modulus or the time coordinates. Also, it is to be noted that the $scG_s(t)$ and $mcFG_s(t)$ curves are very close to each other both at the fast mode and slow mode regions. These

14

comparisons help us to disseminate the contributions from the modified LJ interactions, which contribute to the stress in the fast relaxation regime. We may rename these interactions to be the *inter-segmental interactions* (ISI). The observations suggest that the forces from the ISI (or, modified LJ interactions) fluctuate relatively fast and get averaged out in the long time region, resulting in a mean interactions field for each chain. Indeed, in the long time regime, there are no basic differences in the relaxation behavior between a single chain system and a multiple chain system.

Further, closer examination reveals that in the slow mode region, the $mcTG_s(t)$ curves are consistently closer to the Rouse analytical Rouse$G_s(t)$ curve, than the $scG_s(t)$ and $mcFG_s(t)$ curves. This implies that the inter-segmental interactions have exerted a cohesive influence on the chain dynamics in the long time region; so that the entropic nature of the segmental motion is closely mimicked by the Rouse segment. This effect may also contribute to attest the success of the Rouse theory in explaining the experimental results in the long time region.

3.2. Length scale of the inter-segmental interactions (ISI)

In order to bring out the significance of the length scale on the relaxation behavior, we need to examine the effect of changing the bead diameter on the $G_s(t)$ curves. Figure 2 displays the $mcTG_s(t)$ curves at $\sigma = 0.25$, 0.45 and 0.65 with ε^* fixed at 0.05. For the sake of comparison we also present the full family of curves, namely, $scG_s(t)$, $mcFG_s(t)$ and Rouse$G_s(t)$. It is evident that, at $\sigma = 0.65$, the difference between the $mcTG_s(t)$ (open circles) and $mcFG_s(t)$ (open triangles) curves is most pronounced and the relaxation of the inter-segmental interactions mode covers the fast mode region and a large section of the slow mode region. By contrast, at $\sigma = 0.25$, the range

of the ISI mode does not elongate much beyond the tail part of the fast mode, clearly indicating that the $mcTG_s(t)$ and $mcFG_s(t)$ curves to be identical in the slow mode region, from $t \approx 70$ MC steps onwards (indicated by an arrow). As expected, an intermediate picture emerges for the $\sigma = 0.45$ case.

It is also noteworthy that the full $mcTG_s(t)$ curves at $\sigma = 0.45$ and 0.65 are described by the Rouse theory in the slow mode region, despite a large section (up to ~200 MC steps for $\sigma = 0.45$ and ~1000 MC steps for $\sigma = 0.65$) being much enhanced by the contributions from the ISI mode.
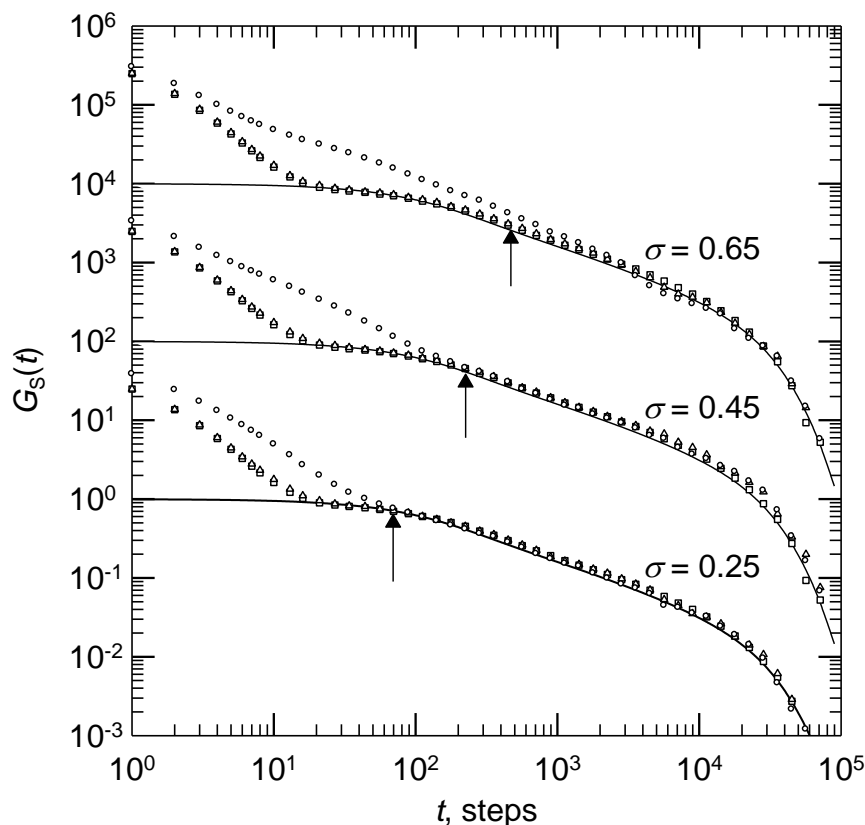
Figure 2: Comparison of the simulation $G_s(t)$ curves at three different $\sigma = 0.25$, 0.45 and 0.65 with $\varepsilon*$ fixed at 0.05. Results for 16 chains × 20 beads, Fraenkel + modified LJ: $mcTG_s(t)$: (O), total force being used in stress calculations; 1 chain × 20 beads, Fraenkel: $scG_s(t)$: (□); 16 chains × 20 beads, Fraenkel + modified LJ: $mcFG_s(t)$: (Δ), only the Fraenkel force being used in stress

calculations. Also shown are the Rouse analytical curves (——) Rouse$G_s(t)$, for $N = 20$. To avoid overlapping, the families of curves at $\sigma = 0.45$ and 0.65 have been shifted vertically by 2 decades and 4 decades, respectively. The arrows indicate the positions of $\tau_f = (\sigma^2/d^2)$.

The exact contributions due to the ISI mode at different σ values can be obtained by subtracting the $mcFG_s(t)$ (using only the Fraenkel force) curves from the $mcTG_s(t)$ (using the total force) curves and these are shown in Figure 3. The results indicate that with increasing bead diameter, the relaxation of the ISI mode becomes much slower with a delayed decrease of the modulus.
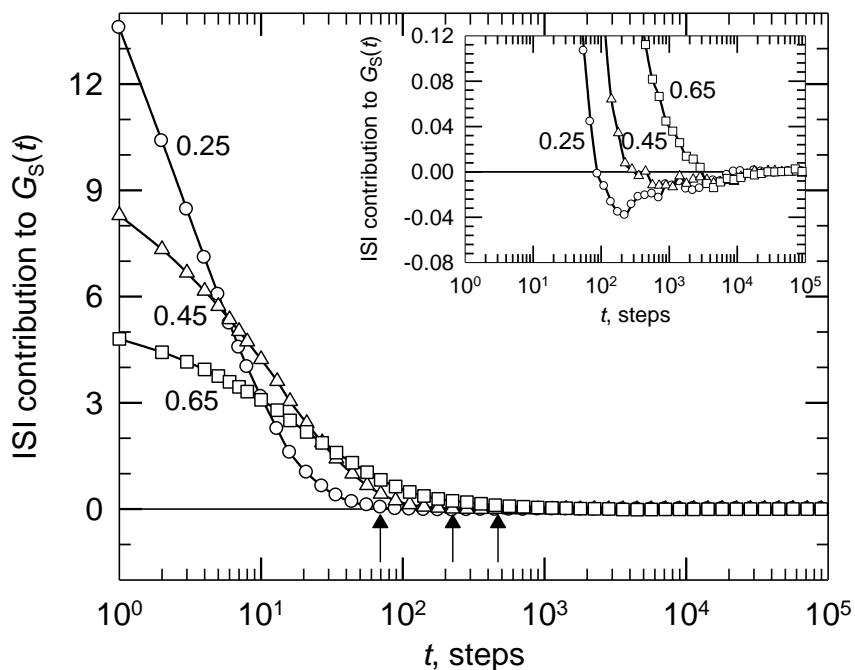

Figure 3: Comparison of the ISI modes for fixed $\varepsilon^* = 0.05$ and at different $\sigma = 0.25$ (O), 0.45 (Δ) and 0.65 ($\square$); as obtained from the plots shown in Figure 2. The arrows indicate the positions of $\tau_f = (\sigma^2/d^2)$. The numbers adjacent to the curves indicate the σ values. The inset shows the small negative values of the ISI modes in their tail parts.

In polymer dynamics, a time scale is associated with a characteristic length scale of the system. The plots in Figure 3 suggest that the bead diameter σ is a representative of such a length scale. As shown in Figures 2 and 3, the ISI mode ends approximately at the time step, $\tau_f = (\sigma^2/d^2)$ (indicated by an arrow) in the cases of $\sigma = 0.25$, 0.45 and 0.65. With the largest σ, the ISI mode extends to somewhat longer times revealing a *crowding effect* (see later) in the polymer system.

3.3. Effect of the well depth parameter ε^*

Figure 4 shows the contributions of the ISI modes at different ε^* obtained by subtracting the $mc\mathrm{F}G_s(t)$ (using only the Fraenkel force) curves from the $mc\mathrm{T}G_s(t)$ (using the total force) curves displayed in Figure 1. After normalization to unit initial modulus (inset B in Figure 4), the three curves of $\varepsilon^* = 0.05$, 0.10 and 0.15 are very close to one another and end at nearly the same time step. In Figure 2, we have demonstrated that by increasing bead diameter σ at a fixed value of ε^*, one can achieve an enhanced $G_s(t)$ accompanied with a longer time scale for the relaxation. Similarly, by increasing ε^* at a fixed value of bead diameter σ, an enhanced $G_s(t)$ results, but with no increase in the time scale for relaxation. A small negative region at the tail part of the ISI mode may be noticed (inset of Figure 3 and inset A of Figure 4) for small σ and large ε^*, which is of no particular importance because of its small magnitude.
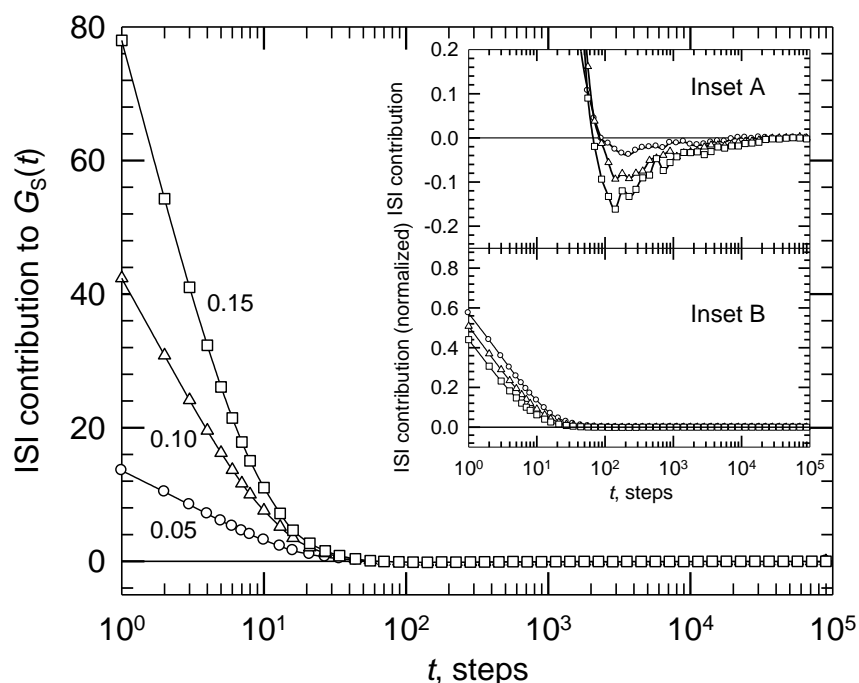
Figure 4: Comparison of the ISI modes for σ fixed at 0.25 and different $\varepsilon* = 0.05$ (O), 0.10 (Δ) and 0.15 ($\square$); obtained from the plots in Figure 1. The numbers adjacent to the curves indicate the $\varepsilon*$ values. Inset A shows the small negative values of the ISI modes in their tail parts. Inset B shows the ISI modes normalized to unit initial modulus.

3.4. Experimental $G(t)$ curves of a nearly monodisperse polystyrene sample

It has been shown that a change in $\varepsilon*$ affects the modulus level (Figure 1) while a change in σ affects both the modulus level and the time scale (Figure 2) of the fast modes in the $mcTG_s(t)$ curves. Interestingly, the slow mode relaxation in the $mcTG_s(t)$ remains well described by the Rouse theory[20] in all aspects; modulus level, time scale and line shape including the N and p dependences of the relaxation times.[20,33,38] Thus, the motion in the slow mode may be interpreted in equivalent terms in the light of the Rouse theory. Following eqs. (5)-(8), using the same d in all the MC simulations implies using the same frictional factor in order to describe the relaxation

behavior of the polymeric system in terms of the Rouse theory.[20] Clearly, all the $mcTG_s(t)$ curves at different ε^* values (Figure 1) can be superposed on each other in the slow mode region without any shift. Experimentally, it is also known that the $G(t)$ curves of an entanglement-free system measured at different temperatures can be superposed on each other over the slow mode region.[6-9,42] In the light of the Rouse theory, making such a superposition also means that the measured $G(t)$ curves are normalized to share the same frictional factor,

$$K = \frac{\xi \langle b^2 \rangle}{k_B T \pi^2 m^2} \qquad (12)$$

where, $<b^2>$ is the square of the segment length, $m = (M/N)$ is the mass of a single bead and M is the molecular weight. Such a set of $G(t)$ curves of the nearly monodisperse polystyrene system, whose weight average molecular weight is equivalent to $N = 20$, have been derived.[42] Since all the MC simulations are performed on ideally monodisperse systems, we make use of the parameters obtained from the $J(t)$ analyses to calculate the $G(t)$ curves with $N = 20$, which are shown in Figure 5.
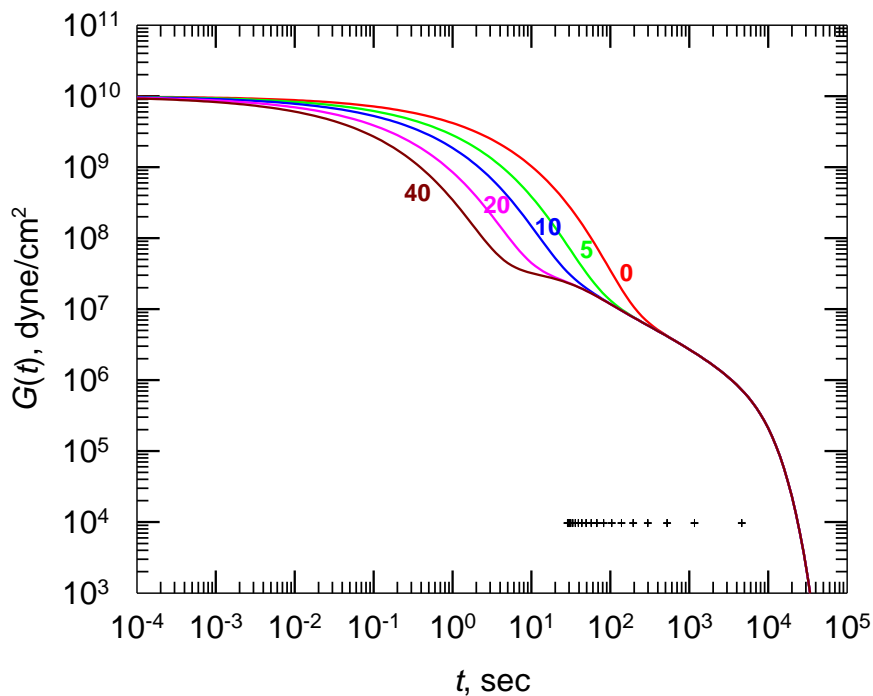
Figure 5: Experimental $G(t)$ curves calculated for different temperature differences from the glass transition point; $\Delta T = 40^0$ C, 20^0 C, 10^0 C, 5^0 C and 0^0 C (indicated by the numbers adjacent to the curves) for an ideally monodisperse sample with $N = 20$ using the parameters obtained from analyzing the $J(t)$ results of a polystyrene sample (molecular weight 16400, polydispersity index 1.05).[42] Note, the mass of a Rouse segment = 850. The (+) symbols represent the Rouse relaxation times of different modes. All the curves are normalized with respect to the frictional factor $K = 10^{-4}$ and the reference temperature for the modulus is 373 K.

It is evident from the family of curves in Figure 5 that the glassy relaxation region of the $G_s(t)$ curves for smaller ΔT extend to longer times, indicating a stronger temperature dependence of the relaxation process in the fast mode. This makes the monodisperse polystyrene sample to be thermorheologically complex. Earlier, we have defined the well depth parameter in the modified LJ potential as, $\varepsilon^* = \varepsilon/(k_B T)$. Thus, a lower temperature means a larger ε^* and vice versa. With decreasing temperature the well depth parameter in the LJ potential becomes larger. As the density

of the polymer system increases, there is enhanced cooperativity in various modes of motion.[43,44] In the light of the inverse relation between ε^* and T, one can superpose the $mcTG_s(t)$ curves at ε^* = 0.05, 0.10 and 0.15 (Figure 1) on one other in the slow mode region. This can be viewed as equivalent to the experimental results at different temperatures being superposed on one another over the slow mode region (Figure 5). Then an increase in ε^* causing an enhancement in the modulus level of the fast mode is equivalent to a decrease in system temperature. As a consequence, the glassy relaxation process gets extended to longer times. However as seen in Figure 4, an increase in ε^* alone is not enough to cause the modulus change and time scale change in the $mcTG_s(t)$ line shapes. We also need to incorporate a simultaneous increase in the length scale (increase in σ) in reproducing the experimental $G(t)$ curves.

3.5. Simulation of the thermorheological complexity

For the MC simulations on the multiple chain systems, the computations of the $G_s(t)$ curves are strongly dependent on the choice of ε^* and σ, affecting the modulus, time scale and length scale. As these two simple structural units (ε^* and σ) are coarse-grained in nature, a perfect collective description of the experimental $G(t)$ curves over the whole time range is not expected. The MC simulations mimicking the experimental curves need to be judged with such a perspective.

The generation of the $mcTG_s(t)$ curves by MC simulations proceeds in the following way. First, we focus on the fast mode region, as changes in ε^* and σ do not greatly affect the close agreement at the slow mode region. Considering the coarse-grained nature of the two structural units, the priority is first to seek a close agreement between the simulation and experiment over the tail part of the fast mode. Guided by the ISI contributions to the $G_s(t)$ (Figure 2 and 3), the bead

diameter parameter σ has a dominating influence in dictating the time scale of the tail part of the fast mode. Thus, using an approximate ε^* value, the σ value is first determined by the close agreement in the tail part of the fast mode. Then, with this σ value fixed, the ε^* value is adjusted to achieve finer agreement between simulation $mcTG_s(t)$ and experimental $G(t)$, over a time range as wide as possible. Further refinement may be achieved by altering the σ value slightly.
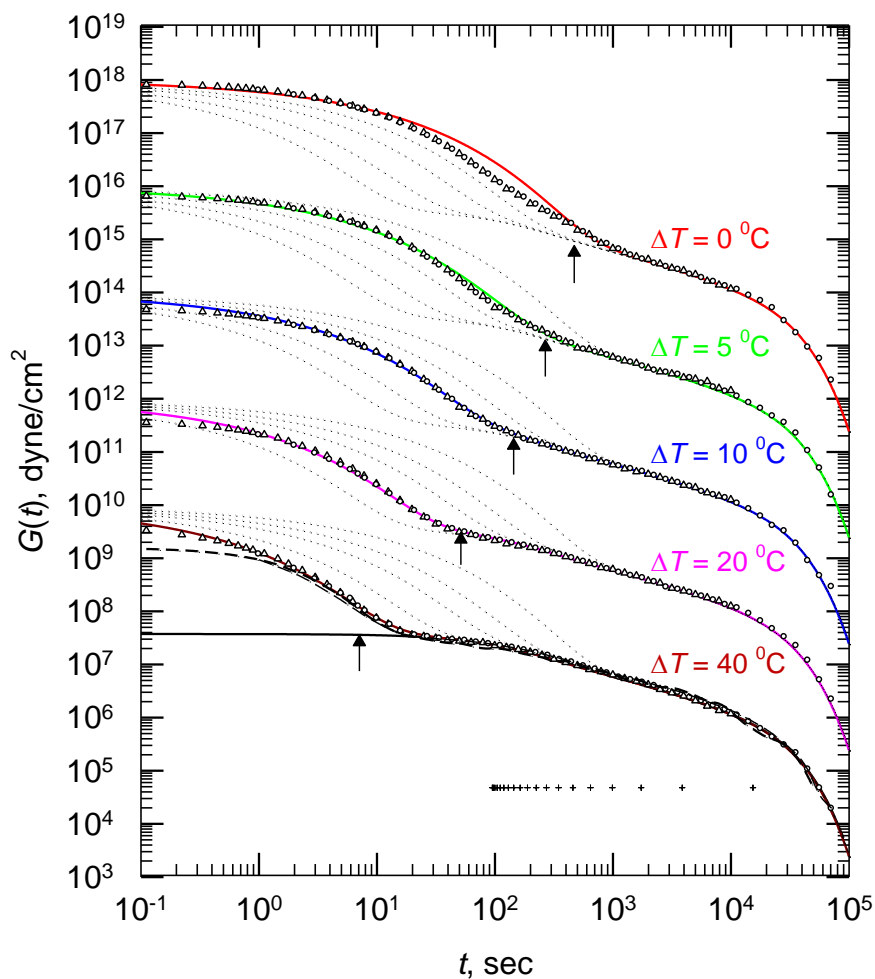
Figure 6: Experiment vs simulation. Simulation $mcTG_s(t)$ curves (points) match with the experimental $G(t)$ curves calculated for the nearly monodisperse polystyrene sample (molecular weight 16400, polydispersity index 1.05) shown in Figure 5. The fitting parameters (σ, ε^*) are: (0.08, 0.03) for $\varDelta T = 40^0$ C, (0.215, 0.075) for $\varDelta T = 20^0$ C, (0.36, 0.15) for $\varDelta T = 10^0$ C, (0.49, 0.22)

for $\varDelta T = 5^0$ C and (0.65, 0.34) for $\varDelta T = 0^0$ C, calculated at a packing fraction 0.5. The simulation results are obtained using, $d = 0.03$ (O) and $d = 0.01$ (Δ).[45] The time coordinate matches with the MC time step based on $d = 0.03$. For comparison, the single Fraenkel chain result, $scG_s(t)$ (---) and the Rouse analytical curve, Rouse$G_s(t)$ (—) are also shown. The simulation data have been multiplied by the shift factor 3.75×10^7 dyne/cm^2 for matching with the experimental $G(t)$. The (+) symbols represent the Rouse relaxation times of different modes. Solid colored lines are the experimental $G(t)$ curves (of Figure 5), each at $\varDelta T$ indicated. To reflect the change of line shapes with temperature, the experimental $G(t)$ curves at $\varDelta T$ values other than the indicated one, are shown as dotted lines. To avoid overlapping, the families of curves at $\varDelta T = 20^0$ C, 10^0 C, 5^0 C and 0^0 C have been shifted vertically upwards by 2, 4, 6 and 8 decades, respectively.

The comparisons of the simulation mcT$G_s(t)$ and the experimental $G(t)$ at different $\varDelta T$ values are shown in Figure 6, for a packing fraction 0.5. We observe that a reasonably good agreement has been achieved between the simulation data and the experimental line shapes. For the sake of comparison, the single Fraenkel chain simulation result, mcF$G_s(t)$ and the Rouse theoretical curve, Rouse$G_s(t)$ are also shown in Figure 6. Despite the coarse-grained nature of the structural units (σ, ε^*), the agreements observed in the cases of $\varDelta T = 40^0$ C, 20^0 C and 10^0 C are amazingly good; slight differences occur only in the very-short-time regions. Except for these negligible differences, the agreements between simulations and experiments over both the fast mode and slow mode regions for $\varDelta T = 40^0$ C, 20^0 C and 10^0 C are quantitatively successful, attesting that the choice of (σ, ε^*) to be optimum for the MC simulations.

It is implicitly assumed that for a viscoelastic sample, the dynamic behavior at length scales above the chosen bead diameter (σ) is ergodic.[46] In the MC simulations reported here, the σ parameter is finite and increases with the decrease in temperature. This implies that some loss of

ergodicity has occurred at length scale smaller than σ. As the temperature gets closer ($\Delta T = 5^0$ C

and 0^0 C) to the glass transition point (T_g), where loss of ergodicity is expected to be more

extensive, the assumption of ergodicity at length scales above σ in the simulations needs to be

verified. This suggests an additional loss of ergodicity is expected at temperatures closer to the T_g.

Despite this presumption, one still sees reasonably good agreements between the simulation data

and the experimental $G(t)$ at $\Delta T = 5^0$ C and 0^0 C. Most importantly, the simulation data are more

than adequate to fully describe the entropic Rouse region at these two temperature differences. The

slow mode relaxation in the long time region maintains its entropic nature even at the glass

transition temperature. This leads to infer that the loss of ergodicity occurring at temperatures close

to the T_g is expected to affect mainly the glassy relaxation in the short time region.

Additionally, in Figure 6, the vertical arrows indicate the positions of $\tau_f = (\sigma^2/d^2)$ for each

of the mcT$G_s(t)$. The fast mode relaxation ends at time τ_f; in other words, the ISI interactions get

averaged out over a time period of τ_f, except for the case of $\sigma = 0.65$, which is due to the crowding

effect. Judging from the τ_f positions ($\tau_f \approx 7, 52, 144, 267$ and 469 MC steps for $\Delta T = 40^0$ C, 20^0

C, 10^0 C, 5^0 C and 0^0 C, respectively) it is clear that the crowding effect[47,48] observed in the

mcT$G_s(t)$ curves with large σ (Figure 2) also occurs at $\Delta T = 5^0$ C and 0^0 C (Figure 6). The said

effect prevents an accurate description of the intermediate part and the tail part of the glassy

relaxation (fast mode) using the MC simulation data, suggesting a limitation of the mcT$G_s(t)$

curves using the (σ, ε^*) values at $\Delta T = 5^0$ C and 0^0 C. An additional loss of ergodicity at length

scales above σ near the T_g results in the crowding effect in the system. Obviously, the disagreement

between the simulation $G_s(t)$ data and the experimental $G(t)$ at the glassy relaxation region reflects

this additional loss of ergodicity at length scales above σ, being ignored in the MC simulations.

As explained above, at temperatures close to T_g, the trajectories of the segmental motion in real systems at the glassy relaxation region are expected to be quite different in terms of ergodicity. However, such nonergodic movements may lead to the expected Rouse behavior in the entropy driven region (in the slow mode), when the ergodicity is recovered.[19] Such an analysis of the recovery of ergodicity has been presented by Sillescu[49] in the case of a dynamically heterogeneous glass forming system at temperatures close to the T_g. According to this analysis, a system may be heterogeneous and nonergodic at times less than a second, but becomes perfectly homogeneous and ergodic on a time scale of hours. This picture emerges naturally in the case of the $mcTG_s(t)$ curves at $\Delta T = 5^0$ C and 0^0 C (Figure 6).

We now present the optimized values of (ε^*, σ) used in the matching of the $mcTG_s(t)$ curves with the experimental $G(t)$ curves in Figure 7.
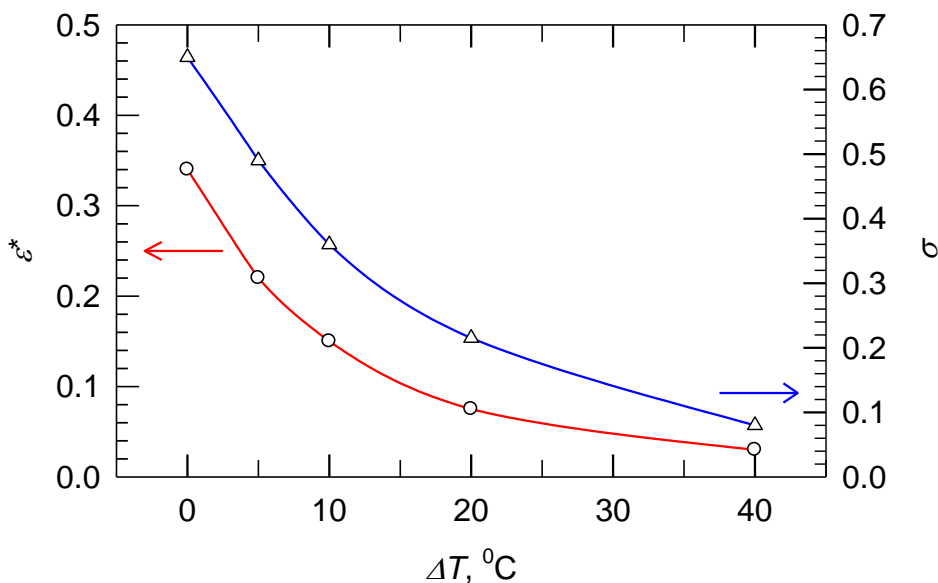

Figure 7: The optimized values of ε^* and σ as a function of ΔT obtained from the matching of the $mcTG_s(t)$ curves with the experimental $G(t)$ curves. Colored arrows indicate the ordinate scales (red for ε^*, blue for σ).

As temperature decreases to approach the T_g, both ε^* and σ increase in magnitude. While an increase in ε^* account for an increase in the relaxation modulus, an increase in σ brings in two effects, increase in the modulus and an increase in the length scale for the glassy relaxation. The increase in the length scale is generally estimated by monitoring the structural relaxation time with respect to the relaxation times of the Rouse normal modes of motion (in the entanglement-free cases) or the Rouse-Mooney normal modes of motion (in the entangled cases).[38]

3.6. Correlation between stress and segmental orientation: Verification of the modified stress-optical rule (MSOR)

Following the application of the step deformation, the polymeric material exhibits anisotropic behavior in stress as well as in refractive index. For the polymeric system, the measured birefringence (resulting from the variations in the refractive index due to anisotropy) is directly proportional to the stress and the relation is known as the stress-optical rule. The modified stress-optical rule (MSOR), which incorporates the deviations at short times, can be written as,[10,11]

$$G(t) = G_G(t) + G_R(t) \tag{13a}$$

$$M(t) = C_G G_G(t) + C_R G_R(t) \tag{13b}$$

where, $G_G(t)$ is the glassy modulus, $G_R(t)$ is the rubbery (plateau) modulus, $M(t)$ is the birefringence and C_G and C_R are the stress-optical coefficients. Mechanical stresses can be interpreted in terms of anisotropies in molecular orientations. Hence, in the multiple chain system, one expects the stress modulus to be proportional to birefringence, in short as well as in long times. For a polymeric system, the orientational tensor of a bond segment **b** can be conveniently defined as,[50,51]

$$S_{\alpha\beta} = \langle b_{\alpha}b_{\beta}\rangle - \frac{1}{3}\delta_{\alpha\beta} \qquad (14)$$

where α, β are the Cartesian components ($\equiv x$, y, z) of the bond segment vector and $\delta_{\alpha\beta}$ is the Kronecker's delta. In order to examine the validity of the MSOR,[10,11,29,52] we have monitored the function $\langle b_x(t)b_y(t)\rangle$ of the 16 chains $\times$ 20 beads system, under step-shear deformation, $\lambda = 0.2$. The ISI parameters ($\sigma = 0.36$, $\varepsilon^* = 0.15$) correspond to $\Delta T = 10^0$ C of the monodisperse polystyrene sample ($M_w = 16400$). In order to match with the simulation $mcTG_s(t)$ curve, the function $\langle b_x(t)b_y(t)\rangle$ needs to be multiplied with the appropriate factors to obtain the glassy modulus, $G_G(t)$ and the rubbery (plateau) modulus, $G_R(t)$. Figure 8 presents the results for $\lambda = 0.2$ at $\Delta T = 10^0$ C. It is evident that $G_G(t)$ is associated with the fast mode and $G_R(t)$ is the counterpart representing the slow mode. The matching of the $mcTG_s(t)$ curve with $C_G\langle b_x(t)b_y(t)\rangle$ in the fast mode and with $C_R\langle b_x(t)b_y(t)\rangle$ in the slow mode yielded the values of the stress-optical coefficients, C_G and C_R, respectively. The values are: $C_G = 9.5 \times 10^{-11}$ Pa^{-1} and $C_R = 1.2 \times 10^{-8}$ Pa^{-1}. In addition, the calculated first normal stress difference, $N_1(t)$ is positive implying that there is a higher degree of orientation in the direction of flow (Figure S1 in the Supporting Information). The second normal stress difference, $N_2(t)$ is about 3 to 10 times smaller than $N_1(t)$ and mostly negative in sign (Figure S2 in the Supporting Information).[28,53,54]

The magnitudes of the C_G and C_R estimated through step-shear simulations modestly differ from the reported values for polystyrene[10,11] [$C_G = 3.2 \times 10^{-11}$ Pa^{-1} and $C_R = -5.0 \times 10^{-9}$ Pa^{-1}]. We attribute the differences due to the following reasons: (1) The measured Young's modulus and birefringence data by Inoue et al[10,11] at several temperatures cover a range of 10^{-4} sec to 10^{+7} sec in time (11 decades), while our MC simulation data (Figure 6) attempt to match the experimental $G(t)$ curves in a much shorter time window (only 6 decades, from 10^{-1} sec to 10^{+5} sec). Even for

this shorter time window, we notice that small discrepancies do exist in the matching between experimental $G(t)$ and simulation $G_s(t)$ at shorter times (< 1 sec). Thus, Inoue *et al*'s data are more accurate and the MC simulation data reported here are only of generic nature. (2) We have chosen a temperature of $\Delta T = 10^0$ C, which is not very far from the T_g. As pointed out by Osaki and Inoue,[52] that the MSOR is valid only approximately and may not be valid even approximately, for polymers with low stress-optical coefficients. Moreover, the validity of the stress-optical law holds for single-phase melts and entangled solutions, that are well above their glass transition temperatures, as long as the chain deformation is not so large so as to be treated as nonlinear.[55-57] (3) Our choice of $\lambda = 0.2$ for the step-shear deformation is somewhat arbitrary, which may not precisely meet the linearity requirement as stated in (2). (4) In the present context, the origin of the negative value of the C_R coefficient lies in the much wider time scale employed in the birefringence experiment,[10,11] which are not accessed by the MC simulations in this work. When we match the full $mcTG_s(t)$ curve with $C_R<b_x(t)b_y(t)>$ in the slow mode for a much shorter time window, there are no occurrence of a negative value of the C_R. This requires further investigations for confirmation.
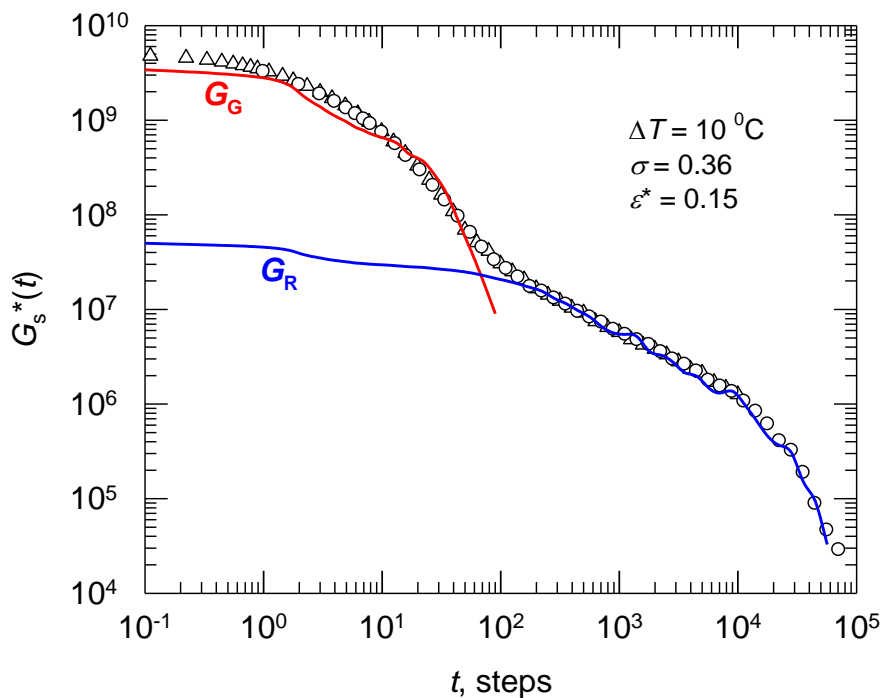
Figure 8: Modified stress-optical rule illustrated by the simulation $mcTG_s(t)$ curve of the 16 chains $\times$ 20 beads system, using $\sigma = 0.36$ and $\varepsilon^* = 0.15$ (corresponding to $\Delta T = 10^0$ C of the monodisperse polystyrene sample of $M_w = 16400$). The simulation data (open triangles and circles) have been multiplied by the shift factor 3.75×10^7, hence the ordinate is named as $G_s^*(t)$. Following the step-shear deformation, the bond segmental anisotropy was monitored by the function $<b_x(t)b_y(t)>$, where $b_x(t)$ and $b_y(t)$ are the x- and y- components, respectively, of the bond segment vector. The red curve is the $G_G(t)$ ($\equiv$ modulus of the glassy state) and the blue curve is $G_R(t)$ ($\equiv$ modulus of the rubbery state). $G_G(t)$ has been obtained as $C_G^*<b_x(t)b_y(t)>$, for $1 \le t \le 100$ MC steps, while $G_R(t)$ has been obtained as $C_R^*<b_x(t)b_y(t)>$, for the entire time range. The estimated values of C_G and C_R are 9.5×10^{-11} Pa^{-1} and 1.2×10^{-8} Pa^{-1}, respectively.

3.7. Mean interactions field formed by the modified LJ potential

We now show the nature of the modified LJ potential function defined in eq. (2) using the optimized ε^* and σ values from the matching of the $mcTG_s(t)$ curves with the experimental $G(t)$ curves. Figure 9 displays the potential functions for $\Delta T = 40^0$ C, 20^0 C, 10^0 C, 5^0 C and 0^0 C. In

30

order to avoid the singularity at $r = 0$, we have used a left cutoff at 0.9σ for all the potential functions.
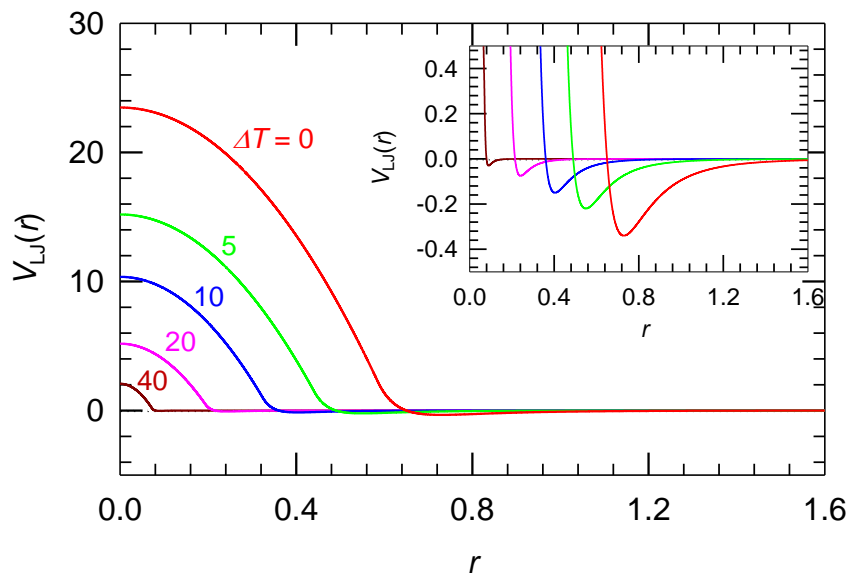

Figure 9: The modified LJ potential functions calculated using the optimized values of ε^* and σ at $\Delta T = 40^0$ C (dark red), 20^0 C (pink), 10^0 C (blue), 5^0 C (green) and 0^0 C (red) obtained from the matching of the $mcTG_s(t)$ curves with the experimental $G(t)$ curves. The inset shows a blowup of the region around $V_{LJ}(r) = 0$.

The introduction of the left cutoff in calculating the LJ interactions in the MC simulations has become necessary because the random step movement d [in eqs. (5)-(8)], along with the total force on the bead, decides the next step position of each bead. As the segments and beads used in the MC simulations represent structural units much larger than the atoms involved in the MD simulations, the time scale corresponding to the step length d is much longer than the typical time step (~ 1 to 5 fs) employed in MD simulations. Because of these differences, the LJ or the modified LJ form of the potential cannot be used in the MC simulations without avoiding numerical blow-ups in the computations. Conventionally, a coarse-grained structural unit needs to possess certain

flexibility (i.e., a coarse-grained bead is not synonymous to a rigid impenetrable atom). The LJ or modified LJ form which can properly model the inflexible spherical shape of an atom cannot be used to model a bead representing a chain section in the MC simulations because of the requisite flexibility. This implies that the potential in the core part of a bead cannot be impenetrable (like that in an atom). The core part of the LJ potential for a bead (as shown in Figure 9) thus represents a penetrable resistance to the approach of another bead. This can be demonstrated by monitoring the fluctuations in the distance between a tagged bead from its nearest neighbor, whose identity may change with time. During the monitoring, it may actually occur that a nearest neighbor bead crosses over to the other side of the tagged bead, right through its center. From monitoring such a fluctuation, the probability distributions as a function of the distance between a tagged bead from its nearest neighbor can be obtained. These are displayed in Figure 10. The probability distributions illustrate the penetration effect; at higher ΔT more number of penetrations is expected resulting in a small magnitude of the closest distance between two beads. As ΔT decreases, the magnitude of the closest distance increases, confirmed by the gradual right shift in the probability maximum, from $\Delta T = 40^0$ C to $\Delta T = 0^0$ C (Figure 10).

As internal rotations are the key physical elements for the chain to be flexible, such penetrable resistance can be provided by the potential barriers to the internal rotation modes in a bead equivalent chain section. At low temperatures, the potential barrier is expected to be much higher than the thermal energy. Thus, as ε^* increases (from $\varepsilon^* = 0.03$ at $\Delta T = 40^0$ C to $\varepsilon^* = 0.34$ at $\Delta T = 0^0$ C), the core potential reaches higher magnitudes (Figure 9). The accompanied increase in the bead size σ (from $\sigma = 0.08$ at $\Delta T = 40^0$ C to $\sigma = 0.65$ at $\Delta T = 0^0$ C) suggests enhanced cooperativity involving more number of internal rotation modes of the chains.
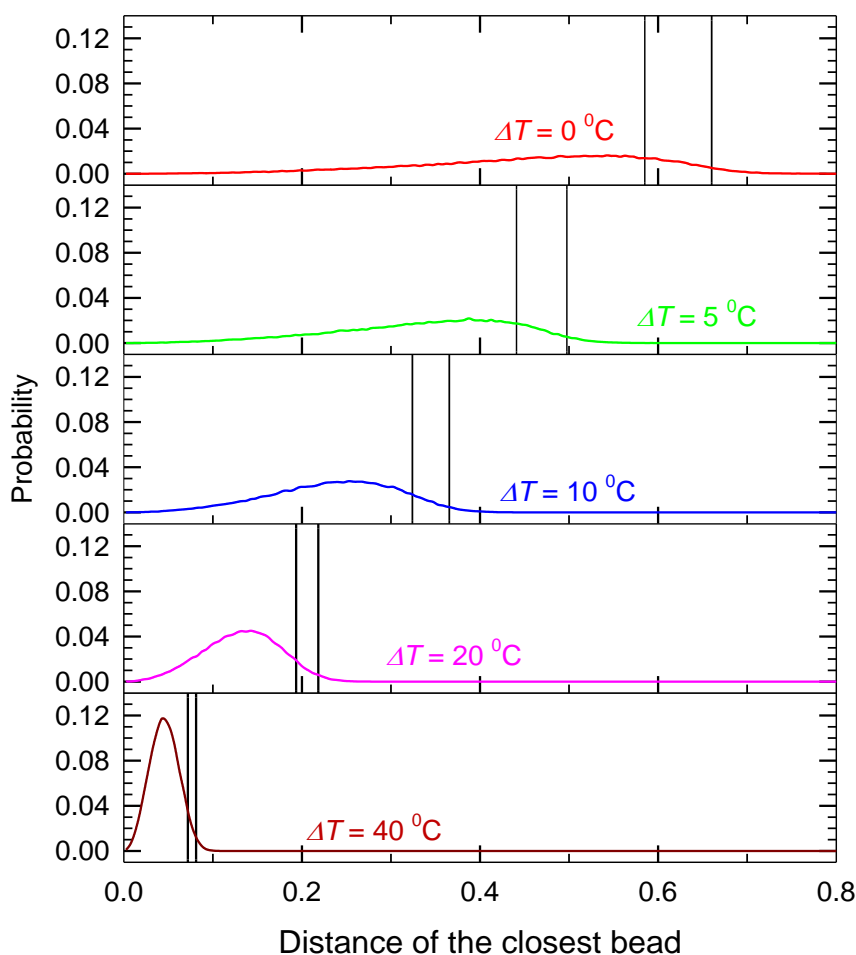
Figure 10: Contours of the probability histograms (with column width set at 0.005) as a function of the distance between a tagged bead (here, the tenth bead in a chain) and its nearest neighbor, corresponding to the modified LJ potentials shown in Figure 9. The left vertical line in each plot represents 0.9σ (left cutoff) while the right vertical line represents the average distance between two beads, defined by $\left(\dfrac{L^3}{cN}\right)^{1/3}$; c is the number of chains, each of N beads, enclosed in a cubic box of edge length L [for example, for the 16 chains $\times$ 20 beads system at $\Delta T = 0^0$ C, bead diameter = 0.65, box length is 4.5148, for a packing fraction of 0.5]. The colored lines are the probabilities for the $\Delta T = 40^0$ C (dark red), 20^0 C (pink), 10^0 C (blue), 5^0 C (green) and 0^0 C (red).

In the Rouse theoretical prescription, the beads in a chain are actually volume-less points. The present MC simulations consider that the LJ beads are penetrable, hence the beads can pass through each other. In addition, segments crossing each other are not ruled out in the MC simulations of the multiple chain systems, a feature also embedded in the Rouse chain model.[20] These are the unphysical events that may not take place in real systems; we encounter these in the simulations, as the involved structural units (ε^* and σ) are much larger than the microstructural length scale. Although a specific functional form of the potential has been given for the inter-bead interactions [eq. (2)], it just represents a mean interactions field for the system under investigation. Specifically, the interaction arising from the presence of a bead on one side of a 'tagged bead' is a part of the mean interactions field at the present time step, just as that due to the bead moving to the other side of the 'tagged bead' at the next time step. The same can be stated about a segment or a chain, before and after crossing each other. Thus, the unphysical event of a bead penetrating through or a chain crossing another chain are all parts of the approximation in the mean interactions field. Because the chain crossing is not forbidden, each chain does not feel the topological constraints due to entanglements and behaves as a topologically independent chain under the mean interactions field. This serves the purpose of our MC simulations for an entanglement-free system.

The MC simulations using the uniform mean field on single Fraenkel chains[27,28] have revealed three important features: (1) the slow mode region is well described by the Rouse theory, (2) the mean squared end-to-end distance is in close agreement with the ideal value, $(N-1)b_0^2$, and (3) the applicability of the virial theorem. In the present multiple chain case, a closely similar time-averaged mean field also leads to the same three features.

In Figure 1 and 2, we have noted the close similarity between the single chain $scG_s(t)$, and the multiple chain (using only the Fraenkel force) $mcFG_s(t)$ curves. (a) This implies that the mean

interactions field experienced by the multiple chain (using only the Fraenkel force), $mcFG_s(t)$ is closely similar to that in the single Fraenkel chain system, $scG_s(t)$. (b) A similar static mean field is indicated by the closeness of the mean square end-to-end distances of the multiple chain system to the ideal value of $(N-1)b_0^2$ for the different sets of ε^* and σ values; the largest deviation being ~10%, occurring at $\Delta T = 0^0$ C, which is attributed to a large value of the bead diameter, $\sigma = 0.65$. (c) The applicability of the virial theorem to the multiple chain system with ($H_F^* = 600$) is also indicated by the calculated average temperature

$$\bar{T} = \frac{-\sum_{k=1}^{c}\sum_{j=1}^{N}\overline{F_{J,k}^{Fraenkel}.R_{J,k}}}{2c(N-1)} = 3.16 \tag{15}$$

being virtually the same as the equivalent quantity in the single-chain case,[27,28] which is in agreement with the virial theorem.

3.8. Dynamical length scale at $\Delta T = 0^0$ C

Being aware of the coarse-grained nature of the structural units (ε^* and σ) involved in the multiple chain system, one may make some rough estimate of the dynamic structural length scale (ς) for the polystyrene system at the T_g. In comparison with the Fraenkel segment, which has some elasticity, the Rouse segment is too soft while the Kuhn segment is totally rigid. With a force constant H_F^* sufficiently large, a Fraenkel segment can be regarded as equivalent to a Kuhn segment as far as chain conformation is concerned. In view of this, the agreement of the simulation data on single Fraenkel chain with the Rouse theoretical prediction over the slow mode region has resolved the paradox in the success of the Rouse segment-based molecular viscoelastic theories.[27,28] To be specific, the molecular weight of a Rouse segment (m) and that of a Kuhn

segment (M_K) are equal.[29] For the polystyrene system, both m and M_K are nearly equal to 850.[29] One may estimate the segment length, $b_s = <b^2>^{0.5}$ corresponding to $m = M_K = 850$, in two different ways. The first is based on the relation

$$b_s = a \left(\frac{m}{M_e} \right)^{1/2} \tag{16}$$

where, a is the entanglement distance and M_e is the entanglement molecular weight. The second one is defined by,

$$b_s = \left(\frac{R_m}{M} \right) M_K \tag{17}$$

where, R_m/M is the ratio of the fully extended end-to-end distance to the molecular weight. Using $M_e = 13500$ and $a = 7.6$ nm for polystyrene, one obtains $b_s = 1.91$ nm from eq. (16).[58] With $R_m/M = 2.38 \times 10^{-3}$ nm for polystyrene,[29] we get $b_s = 2.02$ nm from eq. (17). Both the calculations yield the value of $b_s \approx 2$ nm. Thus, the unit length assigned to the Fraenkel segment, $b_0 = 1$ with $H_F^* = 600$ leads to, $b_s = <b^2>^{0.5} = 1.004 \pm 0.001$ for the different sets of (ε^*, σ), is actually equivalent to ≈ 2 nm for the polystyrene system. Then, the σ value being 0.65 at $\Delta T = 0^0$ C (Figure 7 and 9) is equivalent to a length of about 1.3 nm for polystyrene. From the analyses using the length scales of the Rouse or Rouse-Mooney modes of motion as the yardstick[20-24] supported by the calorimetric estimation results,[59] the length scale (ς) of the glassy relaxation for polystyrene has been estimated to be $\varsigma = 3$ nm[59] at the glass transition point (T_g of the polystyrene sample $= 100^0$ C).[59]

At $\Delta T = 0^0$ C, the range of influence of a bead is large enough to reach two beads simultaneously in a connecting segment, giving rise to an effective blob size which may be estimated as, $(b_s + \sigma) \approx 3.3$ nm. This is the *crowding effect* mentioned in Section 3.5, as the tail

36

part of the ISI mode extends beyond the time step, $\tau_f = (\sigma^2/d^2)$, in the case of $\sigma = 0.65$ (Figure 2

and 3). The crowding effect has also been detected in the case of $\Delta T = 0^0$ C, shown in Figure 6.

Thus, in the MC simulations, we are able to *roughly* estimate the dynamical length scale to be, ς

$\approx (b_s + \sigma) \approx 3.3$ nm at the T_g.

The cooperatively rearranging regions (CRR) theory of Adam and Gibbs,[60] predicts a gradual

increase of the length scale with decreasing temperature towards the T_g. As the glass transition is

approached, increasingly larger regions of the material are required to move simultaneously to

permit flow. Quantitative estimation of the size of these regions have been reported by Berthier *et*

al.[61,62] Through their novel multipoint dynamical susceptibility measurements done on several

molecular glass formers and colloids, these authors found that the dynamic susceptibilities display

a peak at the average relaxation time, whose height increases when the dynamics slows down. This

is considered to be a direct evidence of enhanced dynamic fluctuations and a growing dynamic

length scale (ς) near the T_g.[61] The height of the peak in the dynamic susceptibility yields a direct

estimation of the correlation volume, $V_{\text{corr}} = (\varsigma/a)^3$, where, a is the molecular size ($\equiv$ 'bead' size)

of the glass former. This correlation volume is required to be evaluated using Δc_p or c_p [here, c_p is

the constant pressure specific heat, expressed in units of k_B per 'bead'; k_B is the Boltzmann

constant]. The space-time correlations in glass forming liquids may be better understood by

determining the number of molecules that are dynamically correlated (N_{corr}).[62] By analyzing the

relaxation data of a host of supercooled liquids (including glycerol, *o*-terphenyl, salol, propylene

carbonate, *m*-fluoroaniline, propylene glycol, B_2O_3, *m*-toluidine and decaline) obtained from

various experimental studies such as dielectric spectroscopy, dynamic susceptibility, photon

correlation spectroscopy, dynamic light scattering, optical Kerr effect and neutron scattering,

Dalle-Ferrier *et al*[62] have been successful in providing a convincing evolution of the dynamical

correlation, by plotting the $N_{corr,T}$ data of the glass former materials against a 'scaled' time (expressed as the ratio of α-relaxation time divided by τ_0, an arbitrary time of 1ps), when the glass transition is approached. The most interesting observation is that the $N_{corr,T}$ (T_g) data of the different glass-formers are similar (namely, all lie between 8.2 and 15.9). However, one needs to recognize the underlying unresolved puzzle in the experiments performed to study the glass transition, as clearly pointed out in Ref. 62. To be specific, the high precision obtained in the dielectric spectroscopy experiments cannot be matched in other instrumental techniques. In the same spirit, different microscopic observables may or may not be correlated over different length scales.[62]

Following Berthier *et al,*[61] one may now use the $N_{corr,T}$ (T_g) data to roughly estimate the dynamical length scale (ς) of the studied glass formers. The dynamical length scale data are in the range of $2.02a$ to $2.51a$ (where, a is the bead size). In the present work, $a \approx 2$ nm. Thus, the glass forming materials considered by Dalle-Ferrier *et al*[62] will have their dynamic length scales ranging between 4.04 nm to 5.02 nm.

To summarize this subsection on dynamical length scale: the calorimetric estimation yields, $\varsigma = 3$ nm[59] for polystyrene, the MC simulations give a rough estimate as ~3.3 nm for polystyrene, and the value predicted in multiple experiments is 4~5 nm. Such discrepancies in the estimation of ς is not unexpected, considering the difference in precision that exists between probe to probe in experiments and also between numerical simulations vs. experimental evaluations.[62]

3.9. A general picture for polymer viscoelasticity, rheological complexity and glass transition

From the MC simulation study reported in this article, the following overall physical picture emerges for the polymer viscoelasticity. The relaxation modulus $G_s(t)$ curves and the associated thermorheological complexity in a polymeric system are mainly determined by two factors: first, the bead-bead backbone factor, expressed in terms of the Fraenkel segment and characterized by its force constant, H_F^*. Representing the rigidity along the backbone of a polymer chain, H_F^* is mainly related to the force constants associated with the chemical bonds and the bond angles in the microstructure of the polymer. It is the backbone factor that is responsible for the temperature insensitive (i.e., independent of ε^*, σ) framework supporting the coexistence of the energetic interactions driven mode (fast mode) and the entropy driven mode (slow mode). The second is the inter-segmental interactions (ISI) factor, exclusively related to the (ε^*, σ). While the bead-bead backbone factor contains both potential and orientation anisotropy fluctuations, the ISI factor embodies only the potential fluctuations. As a result, both the bead-bead backbone and ISI factors contribute to the glassy (structural) relaxation while the backbone factor alone is responsible for the emergence of the entropic Rouse mode in the long time region. The ISI factor is closely linked to the potential barriers to the internal rotations in a polymer chain. As the temperature decreases towards the glass-transition point, the increase in the length scale and strengthening of the structure embodied in the ISI factor suggest enhanced cooperativeness involving more modes of internal rotation. This means that with decreasing temperature, internal rotation modes may cause retardation to rotation in one another, interlocking the partners to form a region, larger in size and more strongly held together (akin to the formation of dynamical heterogeniety[17,61-64] in the system).

The finite potential height indicating the penetrability of the beads implies that the local structure forming a bead is not permanent. Thus, a bead may be regarded as representing a region of temporarily interlocked isomeric states. This implies that some loss of ergodicity has occurred

at length levels smaller than σ over a time period that is increasingly long with decreasing temperature. The beads in the coarse-grained model that explains the thermorheological complexity represent a structure formed from the interactions among beads, each representing a region of temporarily interlocked isomeric states. Due to the thermal motions of the beads, this structure fluctuates in the presence of a uniform mean interactions field. It is reasonable to assume that the lifetime of the structure is the relaxation time of the ISI mode in the $G_s(t)$. The correlation between the structures vanishes in the long time region, specifically after $\tau_f = (\sigma^2/d^2)$ time steps. Thus, τ_f may be regarded as a time scale associated with the structure corresponding to length scale σ.

At $\Delta T = 0^0$ C, the interlocked structure not only has become large but also its life time has become longer (note, the delayed relaxation of the ISI mode). This may be regarded as a prelude to the extensive loss of ergodicity. Furthermore, severe crowding effect occurs at $\Delta T = 0^0$ C. Hence, although nonergodicity at length scales above σ is absent in the MC simulations, the collective dynamics of the multiple chain system at $\Delta T = 0^0$ C could have produced the kind of physical condition that would invite additional nonergodicity into the system. This embodies the most mysterious physics related to the glass transition phenomenon.

4. Conclusions

Monte Carlo simulations performed on single Fraenkel chains using appropriate force constant for the bead-bead backbone have yielded a two-mode behavior of the shear stress relaxation $G_s(t)$ in homopolymer melts. Using a multiple chain description for the homopolymer

system, in which the inter-segmental-interactions (ISI) are built in, one can obtain nearly accurate $G_s(t)$ curves which can be matched with the experimental $G(t)$ curves, over a wide temperature range around the glass transition region.

The ISI are strongly dependent on the ε^* (well depth) and σ (bead diameter) parameters of the modified Lennard-Jones potential, used for a coarse-grained description of the polymeric system. It has been shown that a decrease in system temperature amounts to an increase in ε^* and vice versa. This concept has been exploited in describing the temperature dependence of the experimentally observed relaxation modulus $G(t)$ line shapes.

The experimental $G(t)$ curves at different temperatures have been mimicked by the MC simulations on multiple Fraenkel chains with the inclusion of the ISI. It has been shown that two important factors dictate the generic behavior in the thermorheological complexity. The first is referred to as the backbone factor and is characterized by the Fraenkel force constant H_F^*. This factor represents the rigidity along the backbone of the polymer chain and is responsible for the coexistence of the energetic interactions driven (fast mode) and the entropy driven (slow mode) relaxations in $G_s(t)$. The second is the ISI factor defined in terms of ε^* and σ. In the normalized time scale, with decreasing temperature, the gradual strengthening of the ISI factor causes the fast mode to extend to the longer times while the slow mode remains unperturbed (described by the Rouse theory). This picture represents the essence of the thermorheological complexity in the homopolymer system.

In addition to the generic behavior of the thermorheological complexity revealed through the simulations, we have also shown the applicability of the modified stress-optical rule (MSOR) by partitioning the typical $G_s(t)$ curves (at a step-shear deformation $\lambda = 0.2$) into glassy and rubbery

components. The simulation $G_s(t)$ data obeyed Inoue-Okamoto-Osaki's MSOR, with different stress-optical coefficients for each of the glassy relaxation and entropic (rubbery) relaxation modes.

With decreasing temperature, the gradual hardening of the ISI factor is indicated by the increase in the bead size σ parameter and increase in the height of the potential (caused by the increase in ε^*) in the core part of the bead. The penetrability of the beads implies that the local structure forming a bead is not permanent. Such finite height of the potential can be provided by the potential barriers to the modes of internal rotation in a bead equivalent chain section. With temperature decreasing towards the glass transition point, a bead becoming harder may be regarded as representing the formation of a region of temporarily interlocked isomeric states. Near the T_g, the fluctuating interlocked structure formed with the characteristic length σ, has a lifetime of $\tau_f = (\sigma^2/d^2)$, when nonergodicity does not occur. As ergodicity is implicit in the MC simulations, nonergodicity at length levels above σ is neglected in the simulations. Such nonergodicity is a very important factor to describe the motion of the beads, when the temperature is just a few degrees away from the T_g. Using this picture, the generic behavior of the thermorheological complexity, which begins to show up at $\Delta T = 40^0$ C in polystyrene melts, can be explained effectively in terms of the two parameters (ε^*, σ).

It may be worthwhile to derive analytical expressions to describe the temperature dependence of the experimental $G(t)$ curves. One such paper has recently appeared[33] in the case of a polymer blend system in the molten state, describing the fast mode as a stretched exponential, slow mode in terms of the Rouse theory and the intermediate time regime has been quantified using a polynomial with several fitting parameters. The unexplained part of the thermorheological

complexity and exact quantification of the nonergodicity in influencing the glassy relaxation behavior need further detailed investigations in the near future, as echoed by Ngai and Plazek in their recent paper.[5]

Appendix I

Effect of the change in H_F on the $G_s(t)$ line shapes of single Fraenkel chains

The single Fraenkel chains studied in Refs. 27 and 28 are equivalent to systems consisting of independent chains formed from coarse-grained structural units in an implicitly assumed mean interactions field. The value of $H_F^* = H_F/(k_B T) = 400$ chosen for the Fraenkel segment had enabled the model to explain successfully the coexistence and relative positions of the fast relaxation and slow relaxation modes in the $G_s(t)$, observed experimentally. Even so, the choice of $H_F^* = 400$ may still be regarded as somewhat arbitrary. In the present MC simulations, the inter-segmental interactions are included, enabling us to simulate the $G_s(t)$ line shapes observed at different temperatures collectively and also to explain the thermorheological complexity in the homopolymer system. In order to achieve a better matching with the experimental $G(t)$ line shapes, one needs to examine the role of changing the value of H_F^* in influencing the $G_s(t)$ data sets in the multiple chain systems.
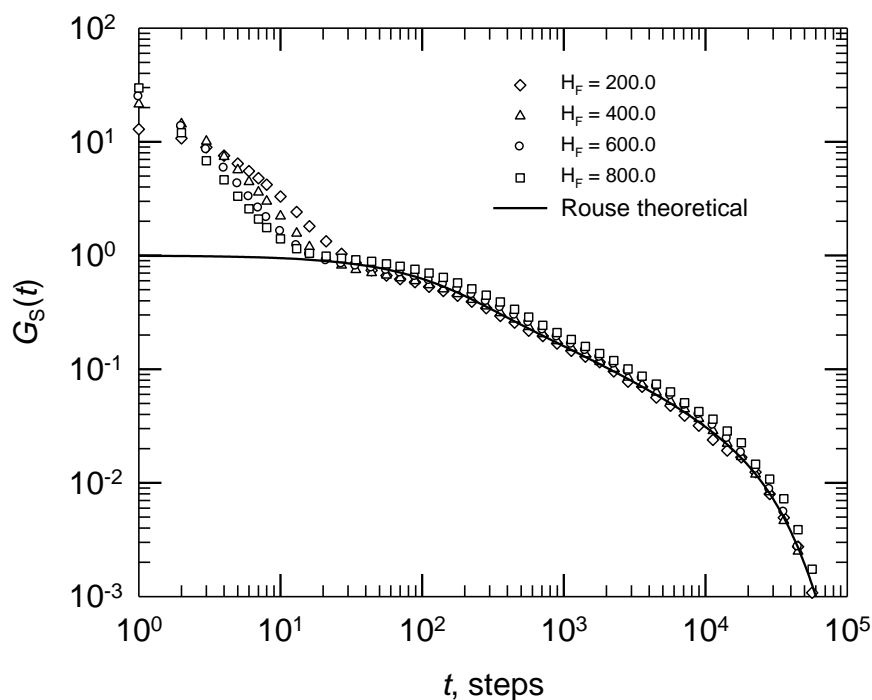
Figure 11: Comparison of the simulation $G_s(t)$ curves of single 20-bead Fraenkel chains with H_F^* = 200 (◊), 400 (Δ), 600 (O) and 800 (□). Also shown is the Rouse theoretical curve (—) for N = 20, without any shift in both modulus and time.

The simulated $G_s(t)$ curves of single 20-bead Fraenkel chains with H_F^* = 200, 400, 600 and 800 are compared in Figure 11. No results for H_F^* larger than 800 are shown; because for H_F^* ≥ 900, the Fraenkel potential becomes too steep for the chosen step length, d = 0.03, causing numerical blow ups in the simulations. Also shown in Figure 11 is the Rouse theoretical curve without any shift in both the modulus and time coordinate. It is evident from the comparison that, both the modulus level and the relaxation time scale of the fast mode are affected by the change in H_F^*. By contrast, only the modulus level of the slow mode is slightly affected by changing the H_F^*. All the four curves superpose closely on the Rouse theoretical curve over the slow mode region by a vertical shift of not more than 10%. In spite of these small differences, the analyses

44

reported in Refs. 27 and 28, identifying the slow mode as an entropic mode remain valid in all of these four cases.

The $G_s(t)$ curve of $H_F^* = 600$ (open circles) appears to be very close to the Rouse analytical curve in the slow mode region without any shift. Furthermore, $H_F^* = 600$ chosen for the present study in the multiple chain system, appears to provide an optimum overall description of the $G_s(t)$ curves at different temperatures when the inter-segmental interactions are included. The trend of small upward shift along the modulus coordinate as N increases from 2 to 5 to 10 to 20 in the case of $H_F^* = 400$ (Figure 3 of Ref. 27) is also observed in the cases of other H_F^* values.

Appendix II

Comparison of equilibrium simulation $G_s(t)$ and step-strain simulation $G_s(t)$

In the single Fraenkel chain cases studied earlier,[27,28] shear stress relaxation modulus $G_s(t)$ curves had been calculated by the MC simulations in the equilibrium state and also after the application of a step-shear deformation at $t = 0$. While the fluctuation dissipation theorem[36] was perfectly demonstrated in the Rouse chain model (Figure 1 of Ref. 27), virtually indistinguishable agreements between the two types of simulations were observed (Figure 7 of Ref. 27) in the Fraenkel-chain model, when N is sufficiently large ($N \geq 10$). In the presently studied multiple chain case, a large discrepancy is observed between these two types of simulations in the fast mode region, while close agreement has been achieved in the slow mode region. This is illustrated in Figure 12 by the comparison of the results of the two types of simulations using the parameters ($\varepsilon^* = 0.15$, $\sigma = 0.36$) for the experimental $G(t)$ curve of $\Delta T = 10^0$ C (Figure 6).
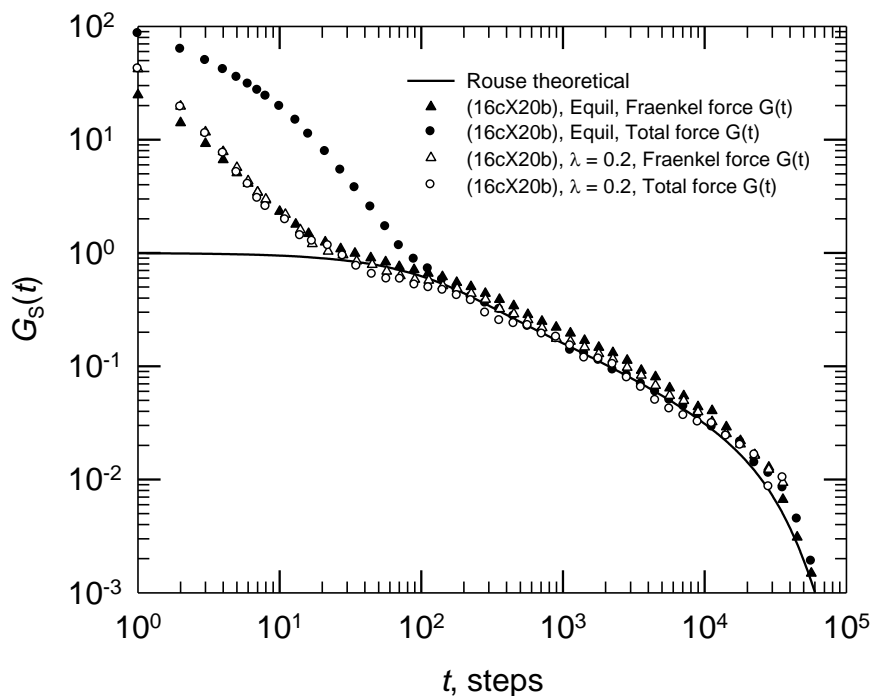
Figure 12: Comparison of the $G_s(t)$ curves [with the $\varepsilon^* = 0.15$ and $\sigma = 0.36$ values for obtaining the $\Delta T = 10^0$ C $mcTG_s(t)$ curve, shown in Figure 6] obtained from simulations in the equilibrium state and following the application of a step-shear strain ($\lambda = 0.2$). Equilibrium simulations: ($\bullet$) for total force being used in stress calculations, ($\blacktriangle$) for only the Fraenkel force being used in stress calculations. Step-strain simulations: (O) for total force being used in stress calculations, (Δ) for only the Fraenkel force being used in stress calculations. Also shown is the Rouse theoretical curve (——) for $N = 20$, without any shift in both modulus and time.

From Figure 12, it is evident from the comparison that, the ISI mode does not contribute to the fast mode in the case of a step-strain simulation. Apparently this is due to the fact that the inter-segmental interactions remain uniformly distributed (like in the equilibrium state) after the application of step-shear deformation. In other words, the configuration distribution associated only with the modified LJ interactions in an equilibrium state is hardly disturbed by the step-shear

deformation at $t = 0$. Furthermore, the mechanism for the ISI mode to occur in the equilibrium simulation may be through a coupling between the Fraenkel and modified LJ interactions as suggested by the existence of the crowding effect (Section 3.5). Supporting such a mechanism is the observation that the ISI mode gets weakened and relaxes faster with the decrease in the bead number per chain (shown in Figure 13), corresponding to the decrease in the average number of Fraenkel segments per bead in the system. Such an effect may contribute to the experimentally observed steep decline in the glass transition temperature of a polymer with decreasing molecular weight in the low molecular weight region (especially, below the entanglement molecular weight).[65-67]
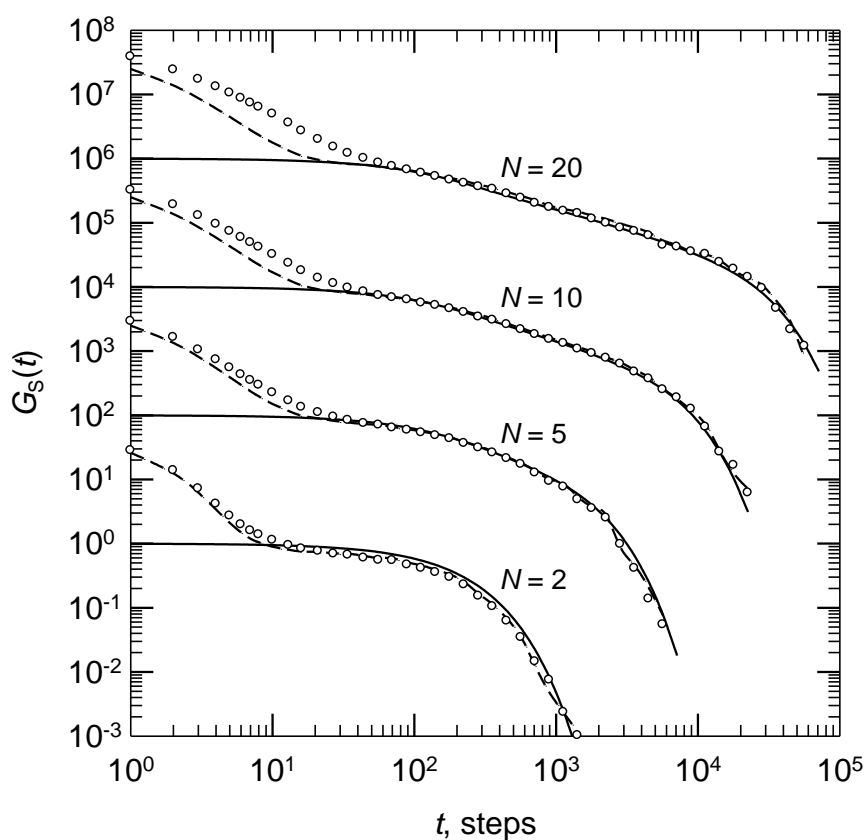
Figure 13: Comparison of the equilibrium simulation $G_s(t)$ curves with $\varepsilon^* = 0.05$, $\sigma = 0.25$ and packing fraction 0.5 for different chain lengths, $N = 20, 10, 5$ and 2. (O) for (16 chains $\times$ N beads),

total force being used in stress calculations; (---) for (16 chains $\times$ N beads), only the Fraenkel force being used in stress calculations. Also shown are the corresponding Rouse theoretical curves (—) for N beads, without any shift in both modulus and time. To avoid overlapping, the families of curves for $N = 5$, 10 and 20 have been shifted vertically by 2, 4 and 6 decades, respectively.

As pointed out earlier (para 2 of this appendix), the coupling between the ISI and Fraenkel interactions is not estimated by the applied step-strain. As a consequence, the ISI mode does not show up in the step-strain simulations. On the other hand, the experimental $G(t)$ curves (compared with the equilibrium simulation $G_s(t)$ curves in Figure 6) are the corresponding relaxation modulus curves obtained following a step-shear deformation. Thus the comparison between the simulation data and the experimental line shapes (Figure 6) has a logical gap corresponding to the differences between the equilibrium and step-strain simulations over the fast mode region. Ignoring the differences between the equilibrium and step-strain simulations for the moment, the present study not only represents the first creation of the thermorheological complexity phenomenon by the MC simulations but also describes the generic effect to a high degree of success. In view of the general equivalence between fluctuations and dissipation, the interpretations based on the successful equilibrium MC simulations should still be valuable.

Acknowledgements

References and Notes

1. I. L. Hopkins, R. W. Hamming; *J. Appl. Phys.* **1957**, *28*, 906.

2. M. Baumgaertel, H. H. Winter; *Rheol. Acta* **1989**, *28*, 511.

3. J. Dealy, D. J. Plazek; *Rheol. Bull.* **2009**, *78*, 16.

4. K. L. Ngai, C. M. Roland; *J. Chem. Phys.* **2013**, *139*, 036101.

5. K. L. Ngai, D. J. Plazek; *Macromolecules* **2014**, *47*, 8056.

6. D. J. Plazek; *J. Phys. Chem.* **1965**, *69*, 3480.

7. D. J. Plazek; *J. Polym. Sci., Part A-2, Polym. Phys.* **1968**, *6*, 621.

8. D. J. Plazek, V. M. O'Rourke; *J. Polym. Sci., Part A-2, Polym. Phys.* **1971**, *9*, 209.

9. K. L. Ngai, D. J. Plazek, I. Echeverria; *Macromolecules* **1996**, *29*, 7937.

10. T. Inoue, H. Okamoto, K. Osaki; *Macromolecules* **1991**, *24*, 5670.

11. T. Inoue, H. Hayashihara, H. Okamoto, K. Osaki; *J. Polym. Sci., Part B, Polym. Phys.* **1992**, *30*, 409.

12. H. Okamoto, T. Inoue, K. Osaki; *J. Polym. Sci., Part B, Polym. Phys.* **1995**, *33*, 417.

13. K. Adachi, H. Hirano; *Macromolecules* **1998**, *31*, 3958.

14. T. Inoue, T. Onogi, M. L. Yao, K. Osaki; *J. Polym. Sci., Part B, Polym. Phys.* **1999**, *37*, 389.

15. M. L. Williams, R. F. Landel, J. D. Ferry; *J. Amer. Chem. Soc.* **1955**, *77*, 3701.

16. T. B. Schroder, S. Sastry, J. C. Dyre, S. C. Glotzer; *J. Chem. Phys.* **2000**, *112*, 9834.

17. P. G. Debenedetti, F. H. Stillinger; *Nature* **2001**, *410*, 259.

18. K. Binder, W. Kob; *Glassy Materials and Disordered Solids*, World Scientific, Singapore,

2005.

19. G. Migliorini, V. G. Rostiashvili, T. A. Vilgis; *Eur. Phys. J. B* **2003**, *33*, 61.

20. P. E. Rouse Jr.; *J. Chem. Phys.* **1953**, *21*, 1272.

21. R. B. Bird, C. F. Curtiss, R. C. Armstrong, O. Hassager; *Dynamics of Polymeric Liquids*,

Volume 2, Second Edition, John Wiley & Sons, New York, **1987**.

22. Y. H. Lin; *Macromolecules* **1984**, *17*, 2846.

23. Y. H. Lin; *Macromolecules* **1986**, *19*, 159.

24. Y. H. Lin; *Macromolecules* **1986**, *19*, 168.

25. G. Williams, D. C. Watts; *Trans. Faraday Soc.* **1970**, *66*, 80.

26. D. Apitz, P. M. Johansen; *J. Appl. Phys.* **2005**, *97*, 063507.

27. Y. H. Lin, A. K. Das; *J. Chem. Phys.* **2007**, *126*, 074902.

28. Y. H. Lin, A. K. Das; *J. Chem. Phys.* **2007**, *126*, 074903.

29. T. Inoue, K. Osaki; *Macromolecules* **1996**, *29*, 1595.

30. G. K. Fraenkel; *J. Chem. Phys.* **1952**, *20*, 642.

31. M. P. Allen, D. J. Tildesley; *Computer Simulation of Liquids*, Clarendon Press, Oxford,

1987.

32. A. K. Das, P. D. Hong; *Polymer* **2010**, *51*, 2244.

33. A. K. Das, D. Y. Hsu, P. D. Hong; *Macromol. Theory Simul.* **2011**, *20*, 19.

34. K. Kremer, G. S. Grest; *J. Chem. Phys.* **1990**, *92*, 5057.

35. M. Bulacu, E. van der Giessen; *J. Chem. Phys.* **2009**, *131*, 064904.

36. D. A. McQuarie; *Statistical Mechanics*, Harper and Row, New York, **1976**.

37. A. R. Leach, *Molecular Modelling: Principles and Applications,* Second edition, Pearson Education Limited, Essex; 2001.

38. Y. H. Lin; *Polymer Viscoelasticity*, Second Edition, World Scientific, Singapore, **2011**.

39. M. Rubinstein, R. H. Colby; *Polymer Physics*, Oxford University Press, Oxford, **2003**.

40. R. B. Bird, C. F. Curtiss; *J. Polym. Sci., Polym. Symposia* **1985**, *73*, 187.

41. R. J. J. Jongschaap; *Rheol. Acta* **1987**, *26*, 328.

42. Y. H. Lin; *J. Phys. Condensed Matter* **2007**, *19*, 466101.

43. J. D. Stevenson, J. Schmalian, P. G. Wolynes; *Nature Physics* **2006**, *2*, 268274.

44. A. Wysocki, R. G. Winkler, G. Gompper; *Europhysics Letters* **2014**, *105*, 48004.

45. For obtaining the $G_s(t)$ values in the MC simulations using step lengths $d = 0.03$ and $d = 0.01$, one needs to run two simulations for the same system: (1) Using $d = 0.03$, for T_{run} MC steps, and (2) using $d = 0.01$, for $9*T_{run}$ MC steps. In the present work, $T_{run} = 10^5$ MC steps. The utility of using a smaller step length value is to access the smaller time scales (Figure 6). The equivalence of using the two different step lengths ($d = 0.01$ and $d = 0.03$) have already been shown earlier [See Figure 2 in Ref. 27]. In Figure 6, the $d = 0.03$ data points are shown as open circles while the $d = 0.01$ data points are shown as open triangles.

46. J. D. Ferry; *Viscoelastic Properties of Polymers*, Third Edition, John Wiley & Sons, New York, **1980**.

47. S. Nakano, D. Miyoshi, N. Sugimoto; *Chem. Rev.* **2014**, *114*, 2733.

48. D. J. Winzor, P. R. Wills; *Biophys. Chem.* **2006**, *119*, 186.

49. H. Sillescu; *J. Noncrystalline Solids* **1999**, *243*, 81.

50. J. U. Sommer, K. Saalwachter; *Macromol. Symp.* **2010**, *291-292*, 251.

51. H. Pleiner, M. Liu, H. R. Brand; *Rheol. Acta* **2002**, *41*, 375.

52. K. Osaki, T. Inoue; *Macromolecules* **1996**, *29*, 7622.

53. R. G. Larson, S. A. Khan, V. R. Raju; *J. Rheol.* **1988**, *32*, 145.

54. E. F. Brown, W. R. Burghardt, H. Kahvand, D. C. Venerus; *Rheol. Acta* **1995**, *34*, 221.

55. C. A. Cathey, G. G. Fuller; *J. Non-Newtonian Fluid Mech.* **1990**, *34*, 63.

56. G. G. Fuller; *Optical Rheometry of Complex Fluids*, Oxford University Press, New York,

1995.

57. R. G. Larson; *The Structure and Rheology of Complex Fluids*, Oxford University Press, New

York, **1999**.

58. L. J. Fetters, D. J. Lohse, D. Richter, T. A. Witten, A. Zirkel; *Macromolecules* **1994**, *27*,

4639.

59. E. Hempel, G. Hempel, A. Hensei, C. Schick, E. Donth; *J. Phys. Chem. B* **2000**, *104*, 2460.

60. G. Adam, J. H. Gibbs; *J. Chem. Phys.* **1965**, *43*, 139.

61. L. Berthier, G. Biroli, J. P. Bouchaud, L. Cipelletti, D. El Masri, D. L'Hote, F. Ladieu, M.
Pierno; *Science* **2005**, *310*, 1797.

62. C. Dalle-Ferrier, C. Thibierge, C. Alba-Simionesco, L. Berthier, G. Biroli, J. P. Bouchaud, F.
Ladieu, D. L'Hote, G. Tarjus; *Phys. Rev. E* **2007**, *76*, 041510.

63. L. Berthier, G. Biroli, J. P. Bouchaud, L. Cipellettei, W. van Saarloos; *Dynamical*

Heterogeneities in Glasses, Colloids and Granular Media; Oxford University Press, New York,

2011.

64. A. Wisitsorasak, P. G. Wolynes; *J. Phys. Chem. B* **2014**, *118*, 7835.

65. R. L. Leheny, N. Menon, S. R. Nagel, D. L. Price, K. Suzuya, P. Thiyagarajan; *J. Chem.*

Phys. **1996**, *105*, 7783.

66. H. Sillescu; *Phys. Rev. E.* **1996**, *53*, 2992.

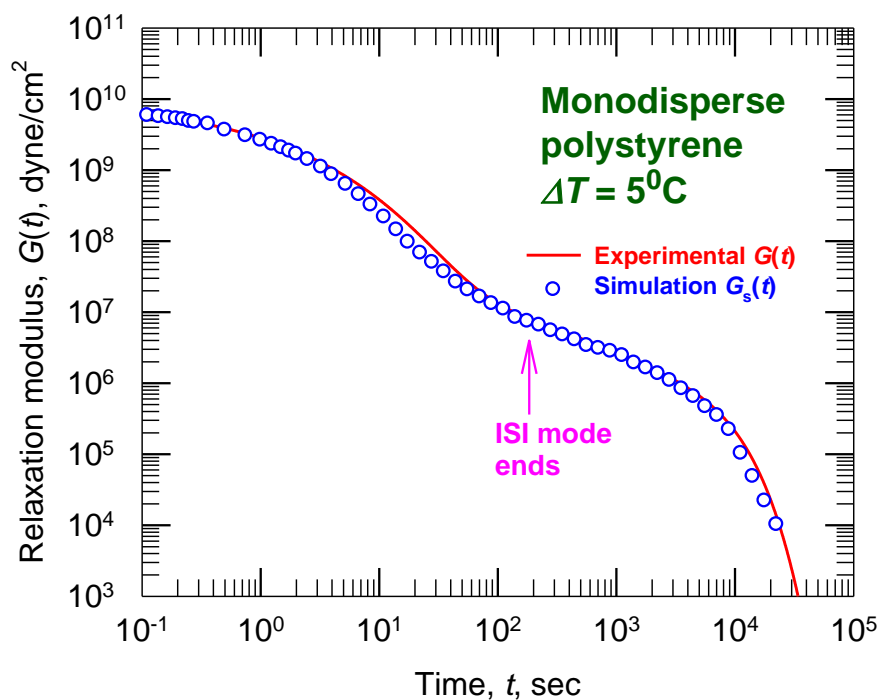67. M. D. Edigar; *J. Noncrystalline Solids* **1998**, *10*, 235.

Table of Contents Page

Exploring the glass transition region: crowding effect, nonergodicity and thermorheological complexity

Ashok K. Das*

**School of Mechanical Engineering
Gyeongsang National University
Jinju, 660701, South Korea.**

Table of Contents Figure

Figure caption: Thermorheological complexity in polystyrene near the glass transition point has been created through Monte Carlo simulations.

Supporting Information

Exploring the glass transition region: crowding effect, nonergodicity and thermorheological complexity

Ashok K. Das*

School of Mechanical Engineering
Gyeongsang National University
Jinju, 660701, South Korea.
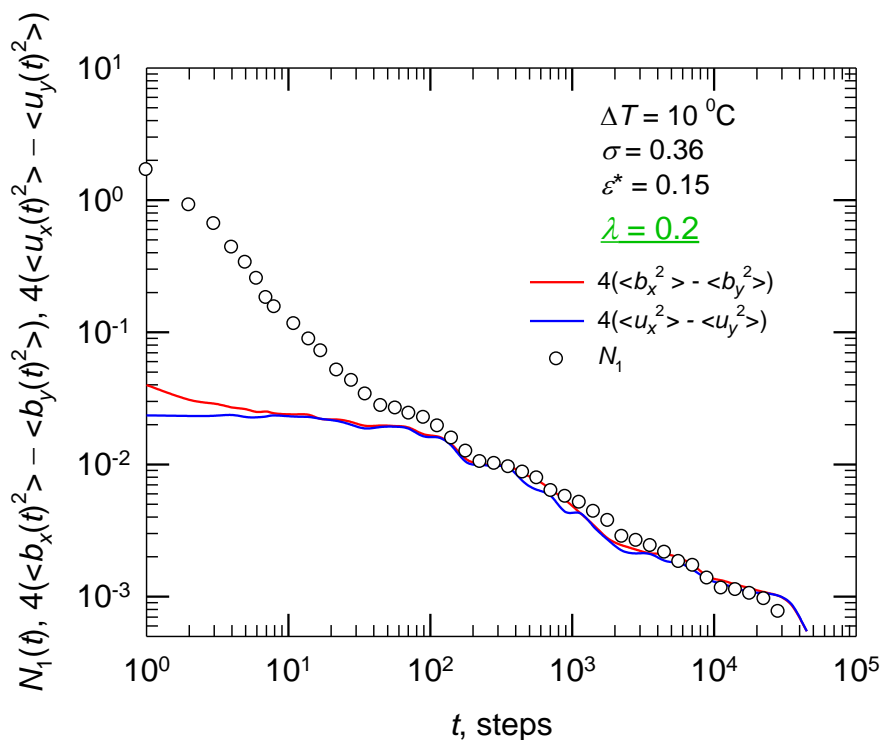
Figure S1: Time dependences of the first normal stress difference, $N_1(t)$ (open circles), $4(<b_x(t)^2>$ $- <b_y(t)^2>)$ (red curve) and $4(<u_x(t)^2> - <u_y(t)^2>)$ (blue curve), obtained from the simulation of the 16 chains $\times$ 20 beads system, using $\sigma = 0.36$ and $\varepsilon^* = 0.15$ (corresponding to $\Delta T = 10^0$ C of the monodisperse polystyrene sample), for a step-shear deformation $\lambda = 0.2$. Here, $b_x(t)$ is the x-

component of the bond segment vector and $u_x(t)$ is the corresponding unit vector component. The important feature of these results is that the first normal stress difference is proportional to the corresponding orientation components in the slow mode region, by a factor of 4. This confirms the entropic nature of the slow mode (see text, Section 3.6).
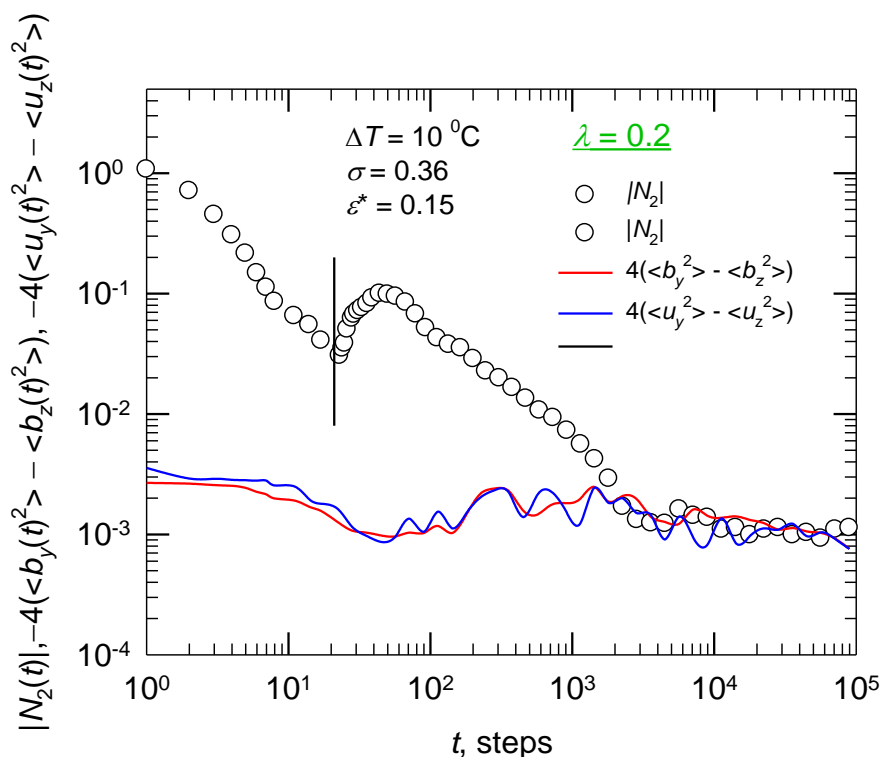

Figure S2: Time dependences of the second normal stress difference, $|N_2(t)|$ (open circles), $4(<b_y(t)^2> - <b_z(t)^2>)$ (red curve) and $4(<u_y(t)^2> - <u_z(t)^2>)$ (blue curve), obtained from the simulation of the 16 chains × 20 beads system, using $\sigma = 0.36$ and $\varepsilon^* = 0.15$ (corresponding to $\Delta T = 10^0$ C of the monodisperse polystyrene sample), for a step-shear deformation $\lambda = 0.2$. Here, $b_y(t)$ is the y-component of the bond segment vector and $u_y(t)$ is the corresponding unit vector component. The vertical line indicates the time step where $N_2(t)$ changes the sign. The important features of these results are: (1) the second normal stress difference is about 1/3 to 1/10 of the first normal stress difference (Figure S1), (2) $|N_2(t)|$ is proportional to the corresponding orientation components in the slow mode region, by a factor of 4, and (3) Negative values of the functions, $4(<b_y(t)^2> - <b_z(t)^2>)$ and $4(<u_y(t)^2> - <u_z(t)^2>)$ indicate that the z-components of the bond segment vector and unit vector are larger in magnitudes. This confirms that the orientation in the y-direction is depleted of polymer orientations relative to the z-direction.